ARTICLES
https://doi.org/10.1038/s41593-017-0012-1

nature neuroscience

Corrected: Publisher Correction

A craniofacial-specific monosynaptic circuit enables heightened affective pain

Erica Rodriguez[1], Katsuyasu Sakurai[1], Jennie Xu[1], Yong Chen[2], Koji Toda[3], Shengli Zhao[1], Bao-Xia Han[1], David Ryu[1], Henry Yin[3], Wolfgang Liedtke[2] and Fan Wang[1*]

Humans often rank craniofacial pain as more severe than body pain. Evidence suggests that a stimulus of the same intensity induces stronger pain in the face than in the body. However, the underlying neural circuitry for the differential processing of facial versus bodily pain remains unknown. Interestingly, the lateral parabrachial nucleus (PB_L), a critical node in the affective pain circuit, is activated more strongly by noxious stimulation of the face than of the hindpaw. Using a novel activity-dependent technology called CANE developed in our laboratory, we identified and selectively labeled noxious-stimulus-activated PB_L neurons and performed comprehensive anatomical input–output mapping. Surprisingly, we uncovered a hitherto uncharacterized monosynaptic connection between cranial sensory neurons and the PB_L-nociceptive neurons. Optogenetic activation of this monosynaptic craniofacial-to-PB_L projection induced robust escape and avoidance behaviors and stress calls, whereas optogenetic silencing specifically reduced facial nociception. The monosynaptic circuit revealed here provides a neural substrate for heightened craniofacial affective pain.

Noxious stimuli experienced by the head and facial region are detected and conveyed to the CNS by sensory neurons located in the trigeminal (TG) ganglia, whereas noxious stimuli affecting extracranial regions are sensed and relayed to the CNS via primary sensory neurons residing in the dorsal root ganglia (DRGs). Humans generally rank head and facial pain as much more severe and emotionally draining than body pain. For example, two of the arguably most severe chronic pain conditions are trigeminal neuralgia and cluster headaches[1–3]. Craniofacial pain sensation is qualitatively different from bodily nociception, as shown in human experiments in which repeated application of noxious heat to the face induces sensitization, yet similar stimulation applied to the hand induces habituation[4]. Fear induced by pain in human subjects was rated higher for face than for extremities, despite comparable ratings of the pain intensity[5]. fMRI studies further revealed that face pain resulted in higher levels of amygdala activation compared to the same intensity of stimulation applied to the hand[6]. Despite these studies, the neurobiological underpinning for heightened craniofacial pain remained enigmatic.

'Suffering' and 'fear of pain' are emotional aspects of pain that are *not* processed by the canonical discriminative pathway via the spino–thalamic–cortical somatosensory circuits. Instead, these feelings are relayed by the less-studied affective pain pathway, where nociceptive afferent information is routed from second-order neurons to the lateral parabrachial nucleus (PB_L) on to various limbic regions, such as the central amygdala (CeA), the bed nucleus stria terminalis (BNST), the lateral hypothalamus (LHA), the anterior cingulate and the insular cortices (also known as the spino–parabrachial circuit)[7–9]. Interestingly, it has been suggested that subregions of the PB_L, a critical relay node in the affective pain circuit, might be differentially activated by noxious stimuli applied to the face versus the extremities in rats[10,11].

In this study, we show that painful stimuli applied to the face activate more PB_L neurons, and do so more bilaterally, than those applied to the paw. We utilize our novel activity-dependent technology, called CANE[12], to identify PB_L-nociceptive neurons and their connections with the affective pain system. We further discover the circuit mechanism underlying the more robust activation of PB_L by noxious facial stimuli and show that activation of this circuit drives strong aversive behaviors, whereas its inhibition specifically reduces craniofacial nociception.

Results

Noxious facial stimuli activate PB_L more robustly and bilaterally than noxious bodily stimuli. We injected 4% formalin (a noxious chemical) unilaterally into either the whisker pad or one hindpaw and then immunostained for expression of the immediate-early gene *Fos* as a marker for activated neurons in the PB_L (Fig. 1a). Whisker-pad formalin injection activated the PB_L, resulting in significantly more Fos^+ neurons than paw injection of an equivalent amount of formalin (Fig. 1c; whisker, 952 ± 100.7, and paw, 616 ± 75.1 total Fos^+ neurons; $P = 0.04$; $n = 7$), especially in the external lateral sub-nucleus of the PB_L (PB-el) (Fig. 1b). Furthermore, unilateral whisker-pad formalin injection induced Fos^+ neurons in PB-el bilaterally, with a trend of more Fos^+ cell on the ipsilateral side (Fig. 1b,d; contra: 213.8 ± 32.8, and ipsi: 281.5 ± 22.3 Fos^+ neurons; $P = 0.053$; $n = 4$). By contrast, unilateral paw formalin injection preferentially activated the contralateral PB-el, with significantly more Fos^+ neurons on the contralateral than on the ipsilateral side (Fig. 1b,d; contra: 253.3 ± 24.1, and ipsi: 129.7 ± 14.3 Fos^+ neurons; $P < 0.01$; $n = 3$), which is consistent with the fact that spino–parabrachial projection neurons in dorsal spinal cord are known to predominantly send axons to the contralateral side[9,10]. Additionally, consistent with the fact that the affective pain circuit does not discriminate the types of pain[7], we found that capsaicin, formalin, and even the minor pain associated with control injection of saline unilaterally into the whisker pad all activated the PB_L neurons (including neurons in PB-el) as compared to the PB_L neuron activity seen in no-injection controls, with formalin being the most potent in evoking Fos^+ neurons (Supplementary Fig. 1a,b; home cage: 73 ± 26, saline: 421 ± 94,

[1]Department of Neurobiology, Duke University Medical Center, Durham, NC, USA. [2]Department of Neurology, Duke University Medical Center, Durham, NC, USA. [3]Department of Psychology and Neuroscience, Duke University, Durham, NC, USA. *e-mail: fan.wang@duke.edu

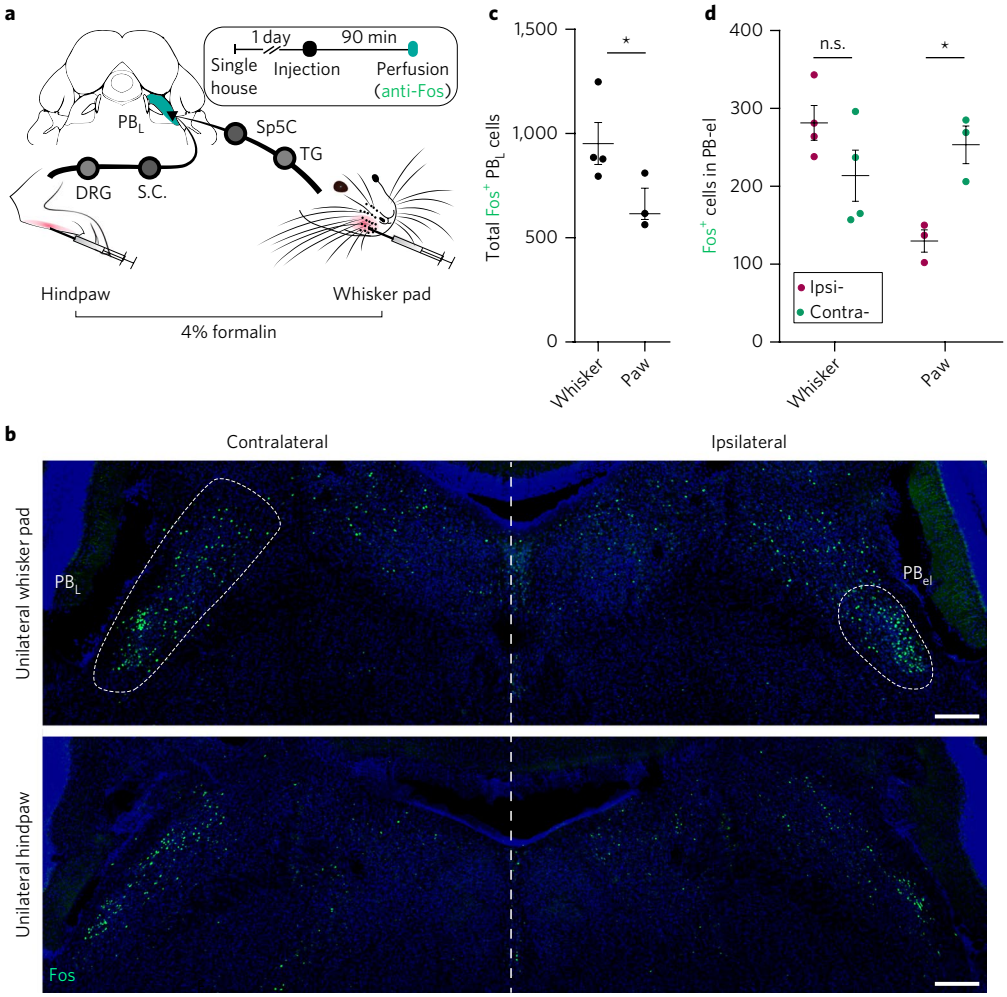

Fig. 1 | Lateral parabrachial nucleus (PB_L) is differentially activated by the same noxious stimulus applied to the face versus hindpaw. a, Schematic illustration of Fos induction protocol. Ninety minutes after 10 µL 4% formalin was injected, brainstem slices containing PB_L were stained for Fos expression. TG, trigeminal ganglion; Sp5C, trigeminal nucleus, caudalis; DRG, dorsal root ganglion; S.C., spinal cord. **b**, Representative images of Fos^+ neurons in PB_L after formalin injection into right whisker pad (top) and right hindpaw (bottom). Large white dashed circle (left) indicates the entire structure of PB_L, whereas small white dashed circle (right) indicates ventral region of PB_L including PB-el. Blue, DAPI stain. Scale bars, 200 µm. **c**, Total numbers of Fos^+ neurons in PB_L on both sides combined ($n=4$, 3; two-tailed unpaired Student's t test; $^*P=0.0445$; $t_{4,962}=2.674$). **d**, Numbers of Fos^+ neurons in ipsilateral (magenta) and contralateral (teal) PB-el in mice unilaterally injected with formalin into one whisker pad ($n=4$) or one hindpaw ($n=3$ mice; two-way ANOVA; whisker: $P=0.0533$; hindpaw: $^{**}P=0.0090$; $F_{1,5}=32.75$). n.s., nonsignificant. Data are mean ± s.e.m.

capsaicin: 673 ± 72, and formalin: 952 ± 101 Fos^+ neurons; $n=3$, 3, 3, 4). In the same animals, we also observed Fos^+ neurons in spinal trigeminal nucleus caudalis (Sp5C), which was expected since Sp5C is a main relay in the trigeminal–thalamic–cortical pain pathway (Supplementary Fig. 1c; $n=3$)[11,13,14].

PB_L neurons activated by noxious facial stimuli are molecularly heterogeneous. Two-color fluorescence in situ hybridization further showed that most *Fos*$^+$ PB_L-nociceptive neurons were *Slc17a6*$^+$ (i.e., *vGlut2*$^+$) (Supplementary Fig. 2a,b; glutamatergic: 80 ± 1%; $n=3$), while only a minority of *Fos*$^+$ cells were *Gad1 Gad2*$^+$ (Supplementary Fig. 2a,b; GABAergic: 7 ± 2%, $n=3$). A recent study showed that the gene *Calca*, encoding calcitonin-gene-related peptide (CGRP), is expressed in PB-el[15]. These $CGRP^+$ PB-el neurons were activated by intense foot shock and transmitted affective pain signals to the CeA[14]. We therefore decided to focus on CGRP expression, and we found that a subset of Fos^+ PB_L-nociceptive neurons in the ventral region indeed expressed CGRP (Supplementary Fig. 2c,d; 56 ± 5% of ventral, 2 ± 1% of dorsal, and 34 ± 3% of total Fos^+ PB_L-nociceptive pain neurons were $CGPR^+$; $n=3$). Another marker, the Forkhead box protein P2 (FoxP2), implicated in circuits related to vocal communication and sodium intake, has also been found to be expressed in the PB_L[16,17]. We found that, again, only a subset of Fos^+ PB_L neurons in the dorsal region expressed FoxP2 (Supplementary Fig. 2c,d; 9 ± 4% of ventral, 46 ± 10% of dorsal, and 21 ± 5% of total Fos^+ PB_L-nociceptive neurons were $FoxP2^+$; $n=3$).

CANE is efficient and selective in activity-dependent capture of facial nociceptive relay PB_L neurons. How might noxious facial stimuli activate more neurons in the PB_L, particularly in the PB-el, compared to noxious bodily stimuli, especially on the ipsilateral side? To answer this question, we needed to identify neurons that provide presynaptic inputs to face-nociception-activated PB_L neurons. Previous studies using anterograde and retrograde tracer dyes labeled the general afferents to the entire PB_L region[9,13,14,18,19]. However, the PB_L contains diverse populations of neurons in addition to neurons responsive to noxious stimuli, such as cells activated by innocuous warm and cool temperatures, as well as cells responsive

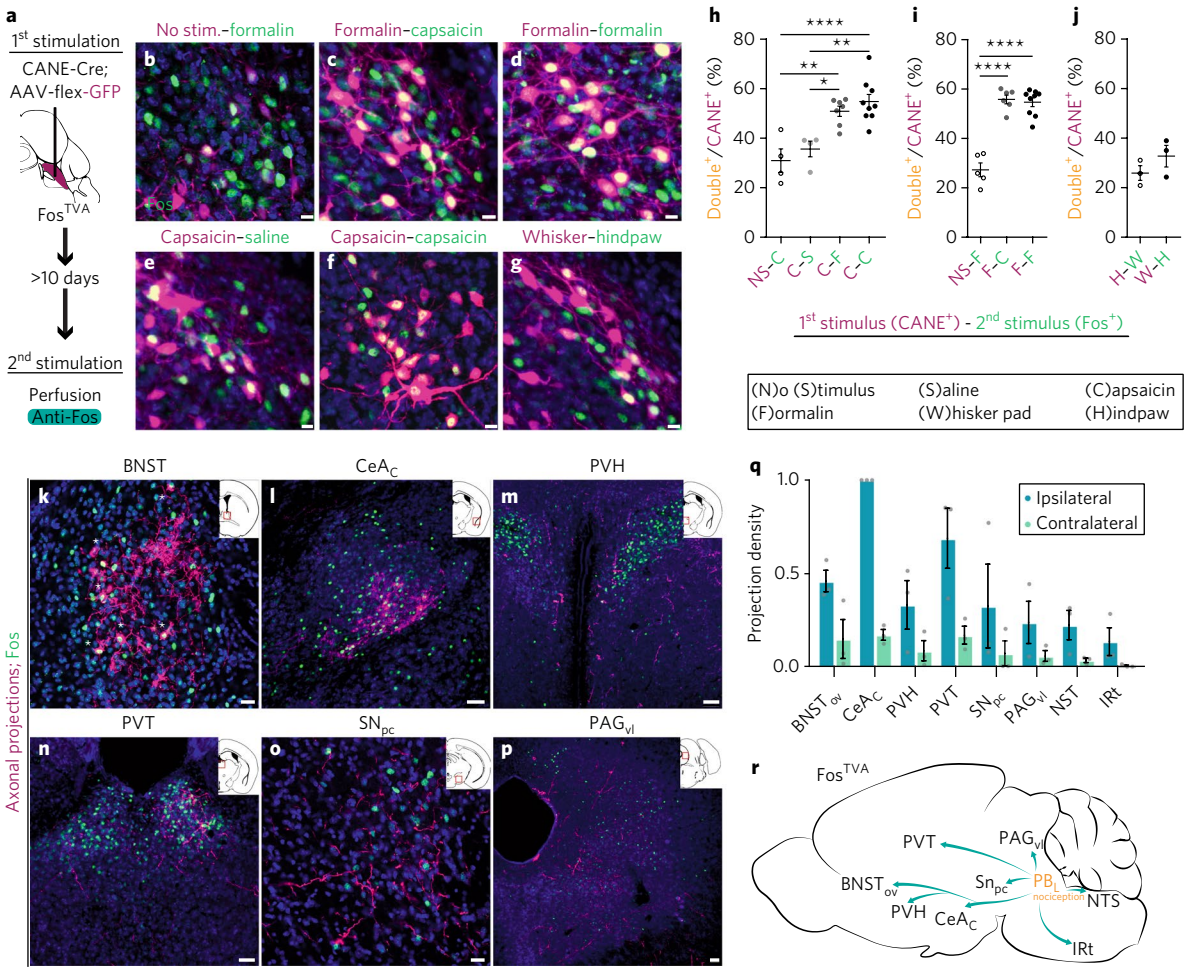

Fig. 2 | Capturing and mapping the axonal projection targets of PB_L-nociceptive neurons. a, Schematic illustration of strategy to express GFP in nociceptive relay PB_L neurons in Fos^{TVA} mice using CANE. **b**–**g**, Examination of CANE-captured neurons activated by the first stimulus (magenta) versus Fos^+ neurons activated by the second stimulus (green) in the PB_L. In all six conditions, CANE method was used to capture neurons activated by stimulus/no stimulus, and 2 weeks later, Fos was induced by the second stimulus. Blue, DAPI. Scale bars, 10 μm. **h**–**j**, The percentages of Fos^+ neurons among $CANE^+$ neurons in the different conditions. Data are mean ± s.e.m. (from left to right: **h**, $n = 4, 9, 7, 4$; one-way ANOVA; $^{****}P \leq 0.0001$, $^{**}P = 0.0005$, $P = 0.3952$, $P = 0.3223$; $^{**}P = 0.0005$, $^{*}P = 0.0047$; $F_{3,20} = 12.49$; **i**, $n = 5, 5, 9$; one-way ANOVA; $^{****}P \leq 0.0001$, $^{****}P \leq 0.0001$, $P = 0.6876$; $F_{2,17} = 52.17$; **j**, $n = 3, 3$; two-tailed unpaired Student's t test; $P = 0.2759$; $t_{3.505} = 1.289$). **k**–**p**, Representative images of axonal projections from captured formalin-activated PB_L (magenta) in several brain nuclei expressing Fos (green) induced by formalin. Insets, schematics of coronal view of location (in red box) in brain. * in **k** denotes very large terminal boutons from labeled PB_L axons in BNST; some of boutons surround the Fos^+ BNST neuron cell bodies. **q**, Quantification of normalized density of innervations (total pixels divided by the area of each nucleus; $n = 3$). All data shown are mean ± s.e.m. **r**, Schematic summary for output targets of PB_L-nociceptive neurons. $BNST_{ov}$, oval nucleus of the bed nucleus of the stria terminalis; PVH, paraventricular hypothalamic nucleus; PVT, paraventricular nucleus of the thalamus; CeA_C, central amygdalar nucleus, capsular part; SN_{pc}, substantia nigra pars compacta; PAG_{vl}, ventrolateral periaqueductal gray; NST, nucleus of the solitary tract; IRt, intermediate reticular tract. Scale bars: **k**,**o**, 20 μm; **l**–**n**,**p**, 50 μm ($n = 3$). Data are mean ± s.e.m.

to various taste stimuli[20,21]. The PB_L is also known for its significant role in regulating instinctive behaviors, namely thirst for water, sodium appetite and hunger for food[22–24]. Thus, tracer-based studies lack the resolution to identify specific inputs to the PB_L-nociceptive neurons. Because CGRP and FoxP2 label only subsets of PB_L-nociceptive neurons (Supplementary Fig. 2c,d), we reasoned that trans-synaptic tracing of inputs to either $CGRP^+$ or $FoxP2^+$ neurons may miss certain types of inputs that innervate the non-$CGRP^+$ and non-$FoxP2^+$ PB_L-nociceptive neurons. We therefore turned to our newly developed technology, CANE, for viral-genetic tagging of transiently activated neurons to capture noxious-stimulus-activated PB_L neurons. CANE uses a pseudotyped lentivirus or rabies virus to selectively infect Fos^+ neurons genetically engineered to transiently express the receptor for the pseudotyped viruses (Fos^{TVA} mice), and consequently, the viruses mediate expression of desired transgenes in activated cells[12].

We first determined whether CANE could indeed selectively label PB_L-nociceptive neurons. In a two-bout experimental paradigm, CANE was used to capture PB_L neurons activated by a noxious stimulus (capsaicin or formalin injection) through co-injection of CANE-LV-Cre and AAV-flex-GFP into the PB_L. Three weeks later, the same animal was given a second painful stimulus to induce Fos expression and was then anesthetized and killed to obtain samples for immunostaining (Fig. 2a). In the capsaicin–capsaicin and formalin–formalin conditions, 55 ± 3% ($n = 9$) and 55 ± 2% ($n = 9$) of CANE-captured PB_L neurons, respectively, were Fos^+ (Fig. 2d,f,h,i). This indicated that the second noxious injection reactivated many (~55%) of the same cells excited by the first stimulus. By contrast, without noxious stimulation, there was only a small number of background captured neurons (due to Fos expression in PB_L induced by handling and restraining the animals even

in the absence of noxious stimuli), which had significantly less overlap with Fos$^+$ neurons induced by noxious stimuli (Fig. 2b,e,h,i; $27\pm3\%$ CANE$^+$ cells were Fos$^+$ in the no stimulus–formalin condition ($n=5$; $P<0.0001$); $31\pm5\%$ CANE$^+$ cells were Fos$^+$ in the no stimulus–capsaicin condition ($n=4$; $P<0.0001$)). In the capsaicin–saline condition, $36\pm3\%$ CANE-captured cells were Fos$^+$ activated by saline injection (Fig. 2e,h; $n=4$; $P=0.0005$), consistent with the fact that saline injection caused only moderate PB_L activation. Previous electrophysiological studies reveal that the same PB_L neurons could be activated by different noxious modalities[25], prompting us to ask whether CANE-captured capsaicin-activated PB_L neurons overlapped with formalin-activated neurons and vice versa. Indeed, we observed a similar percentage of CANE$^+$ neurons that were Fos$^+$ regardless of whether the capsaicin–formalin or the formalin–capsaicin condition was used (capsaicin–formalin: $51\pm2\%$; $n=7$; formalin–capsaicin: $55\pm2\%$; $n=6$) (Fig. 2c,h,i). We also examined the overlap between CANE-captured face-activated PB_L nociceptive neurons and Fos$^+$ cells induced by contralateral hindpaw nociception and vice versa. About 30% of CANE$^+$ neurons were Fos$^+$ in both whisker–hindpaw and hindpaw–whisker nociception paradigms (Fig. 2g,j; whisker–hindpaw: $26\pm3\%$; hindpaw–whisker: $33\pm4\%$, $n=6$ for each condition). Our observations are consistent with the current concept that the PB_L mediated affective pain circuit plays a limited role in discriminating the types and locations of injury[25,26]. As an additional control for the specificity of CANE, we co-injected CANE-LV-Cre, AAV-flex-GFP (CANE::GFP), and AAV-tdTomato into the PB_L after formalin injection into the whisker pad and compared the labeling resulting from the two AAV constructs. CANE::GFP labeled a specific subset of PB_L neurons, whereas AAV-tdTomato labeled a majority of neurons at the injection site (Supplementary Fig. 3; $n=4$), thus further confirming the specificity of our method.

PB_L-nociceptive neurons project axons to multiple emotion- and instinct-related centers in the brain. We next traced the axonal projections of CANE::GFP-captured PB_L-nociceptive neurons. The targets of PB_L nociceptive neurons included the BNST (where PB_L axons form large axonal boutons surrounding BNST neuron cell bodies), the paraventricular thalamic nucleus, the paraventricular nucleus of the hypothalamus (PVH), the capsular division of CeA), the ventral tegmental area, the ventrolateral periaqueductal gray (PAG_{vl}), the nucleus of the solitary tract (NST) and the intermediate reticular nucleus in the hindbrain (IRt) (Fig. 2k–r). Quantitative measurements of the densities of innervation ($n=3$) taken using a previously described method[12,27] showed that the majority of projections were ipsilateral, with small numbers of axons innervating the contralateral side (Fig. 2q). A schematic summary of the projections is shown (Fig. 2r). Notably, all the targets of PB_L-nociceptive neurons contained Fos$^+$ neurons induced by noxious facial stimulation (Fig. 2k–p, green signals).

PB_L-nociceptive neurons receive inputs from emotion-related limbic regions and brainstem nuclei. Having validated that CANE selectively captured PB_L-nociceptive neurons that relay signal to emotion- and instinct-related centers, we mapped the presynaptic inputs to these neurons using a CANE-based trans-synaptic tracing method[12]. Briefly, CANE-LV-Cre and the helper virus AAV-SynP-DIO-TVA-EGFP-RG[28] were co-injected into the ipsilateral PB_L to express the TVA receptor, rabies glycoprotein G and GFP selectively in the PB_L neurons, which were activated by formalin injection into the whisker pad. Two weeks later, CANE-RV-mCherry was injected into the same location in PB_L. The GFP$^+$ mCherry$^+$ double-positive neurons are the starter PB_L-nociceptive neurons, while mCherry$^+$ neurons outside of the PB_L are presynaptic neurons (Fig. 3a,b). We observed mCherry$^+$ neurons in BNST, medial division of CeA, and several hypothalamic nuclei including the PVH, the substantia nigra pars compacta, the PAG_{vl}, brainstem reticular regions, the NST, Sp5C and the dorsal horn of the spinal cord (Fig. 3c–j,m; quantification represents numbers of labeled presynaptic neurons/number of starter neurons; $n=6$). Note that the labeled neurons in the reticular regions, NST and Sp5C were distributed bilaterally with an ipsilateral dominance (Fig. 3m; numbers of trans-synaptically labeled cells/number of starter cell were as follows: ipsilateral: IRt, 6.3 ± 1.3; PCRt, 6.4 ± 1.4; MRn, 1.3 ± 0.4; GRn, 3.1 ± 0.7; NST, 1.9 ± 0.7; Sp5C, 5.3 ± 1.6; and contralateral: IRt, 0.9 ± 0.2; PCRt, 1.4 ± 0.5; MRn, 3.8 ± 0.8; GRn, 2.1 ± 0.5; NST, 0.8 ± 0.2; Sp5C, 0.5 ± 0.2), which is consistent with previous dye tracing studies[9,13,14,18,19]. Additionally, there were a few labeled cells in the contralateral PB_L (Fig. 3m; 0.7 ± 0.2). A schematic summary of the projections is shown (Fig. 3o).

CANE-captured PB_L-nociceptive neurons receive direct inputs from ipsilateral trigeminal ganglion. Interestingly, trans-synaptically labeled mCherry$^+$ neurons were also observed in the ipsilateral TG, but not in any of the DRGs on either side ($n=6$; Fig. 3k,l), suggesting that TG sensory neurons innervating head and face provide direct monosynaptic inputs to ipsilateral PB_L-nociceptive neurons. A few previous anatomical studies hinted at the possibility of a direct TG–PB connection[29–32]. Interestingly, trans-synaptic tracing of inputs to hindpaw formalin-activated PB_L-nociceptive neurons also revealed labeled neurons in TG but not in any DRG ($n=4$; Fig. 3n), suggesting that craniofacial but not body primary sensory neurons provide direct, monosynaptic inputs onto PB_L-nociceptive neurons. The result is also consistent with the idea that some PB_L-nociceptive neurons receive convergent inputs from both face and body. We examined the expression of IB4 (a marker for non-peptidergic C fibers), CGRP, TrpV1 (the receptor for capsaicin and a marker for a subset of C fibers and a small subset of Aδ fibers), and NF200 (a marker for both Aδ and Aβ fibers) among the trans-synaptically labeled TG neurons. The TG neurons directly presynaptic to the PB_L included NF200$^+$ ($45\pm4\%$), TrpV1$^+$ ($38.5\pm4\%$), CGRP$^+$ ($26.2\pm7\%$), and IB4$^+$ cells ($12\pm4\%$; $n=8$; Fig. 3p, q). Taken together, the trans-synaptic tracing studies suggest that there are two separate pathways transmitting craniofacial nociception from TG to the PB_L: (i) the previously known indirect TG→Sp5C→PB_L and (ii) the newly revealed direct TG→PB_L projection. By contrast, there is only one indirect pathway transmitting somatosensory body nociception from DRG to the PB_L: DRG→spinal dorsal horn→PB_L.

Notably, a previous study using TrpV1::PLAP mice observed that fibers from a possible primary afferent source of TrpV1-lineage neurons were present in the PB_L, especially in the PB-el[29,32]. The authors speculated that the TrpV1$^+$ fibers may have emerged from TG neurons, which could provide an alternative circuit contributing to craniofacial pain experience[29,32]. These previous findings, in addition to our finding that ~40% of trans-synaptically labeled TG neurons are TrpV1$^+$, led us to postulate that TrpV1$^+$ fibers may be a major source of noxious TG inputs to PB-el. Therefore, we performed neonatal intraperitoneal (IP) injection of AAV to selectively label periphery-derived TrpV1-Cre$^+$ axons[33–35]. Briefly, Cre-dependent AAV9-flex-GFP was injected into TrpV1-Cre[33] mouse pups at postnatal day 1–2. The IP injection resulted in selective labeling of TrpV1-Cre$^+$ primary sensory neurons with GFP without labeling of TrpV1-Cre$^+$ CNS neurons (Fig. 3r,s and Supplementary Fig. 4; $n=3$). Furthermore, axonal terminals from labeled TrpV1$^+$ primary sensory neurons were observed near nociceptive Fos$^+$ neurons in PB-el and in Sp5C (Fig. 3t; Fos was induced by capsaicin injection into the ipsilateral whisker pad).

We further designed a TrpV1-Cre and retrograde-FlpO intersectional strategy (Supplementary Fig. 5a) to determine whether PB_L projecting TG neurons also project to Sp5C. Briefly, retrograde lentivirus expressing either FlpO (RG-LV-hSyn-FlpO, $n=4$) or Cre-dependent FlpO (RG-LV-hSyn-DIO-FlpO, $n=6$) was injected into

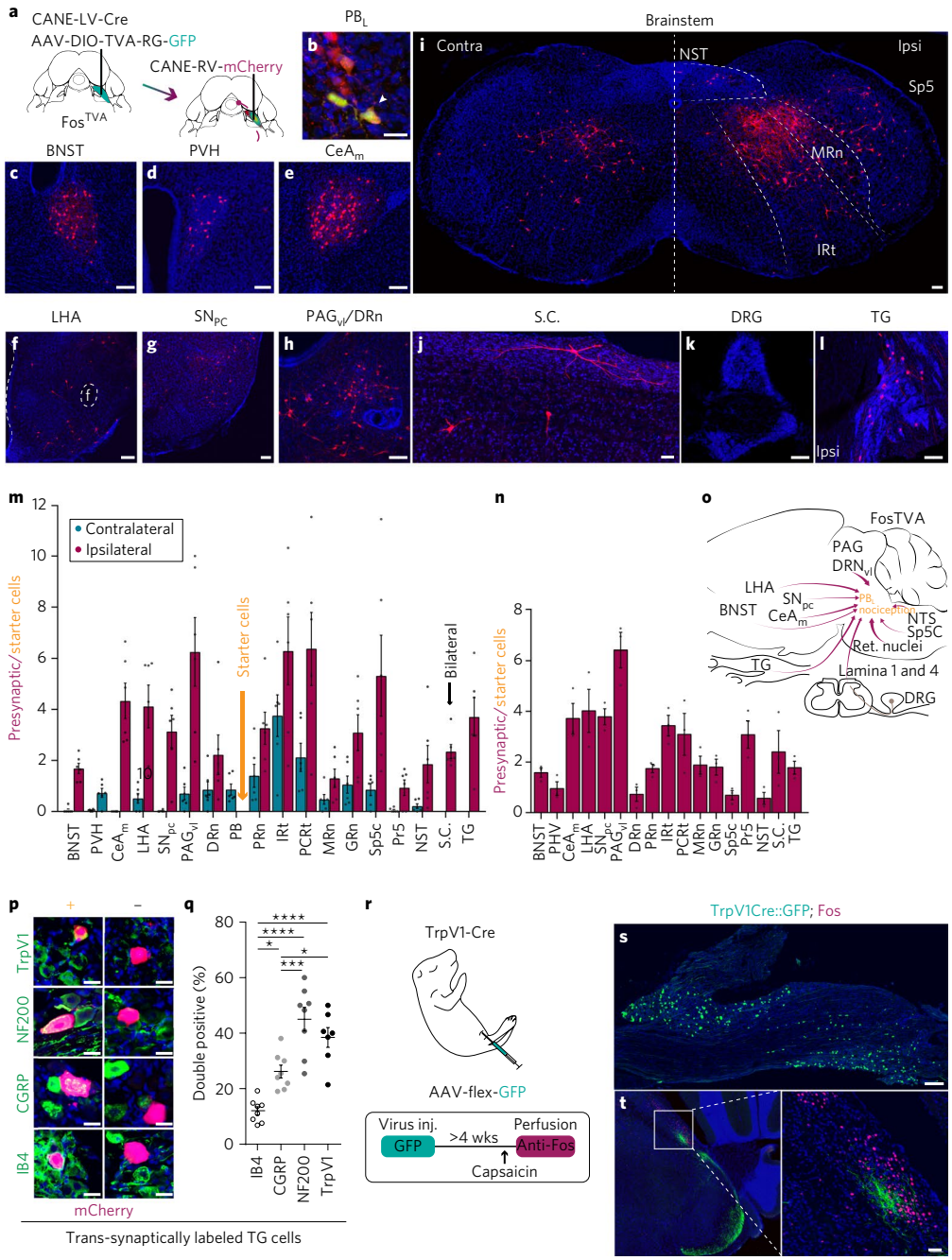

Fig. 3 | Trans-synaptic labeling of presynaptic neurons for PB_L-nociceptive neurons reveals the direct TG→PB_L pathway. a, Schematic illustration for trans-synaptic tracing of presynaptic inputs to PB_L-nociceptive neurons. **b**, Representative image of CANE-RV-mCherry-infected PB_L-nociceptive neurons. Green, PB_L-nociceptive neurons expressing TVA and RG; red, RV-mCherry$^+$; yellow, starter cells. Scale bar, 10 µm. **c**–**l**, Representative images of trans-synaptically labeled neurons in several brain regions. Scale bars: **c**–**h**,**k**,**l**, 50 µm; **i**, 100 µm; **j**, 20 µm. **m**,**n**, Quantification of trans-synaptically labeled neurons in each brain area contralateral (teal) and ipsilateral (magenta) to injected site (**m**) after whisker-pad formalin injection and (**n**) after hindpaw formalin injection. The value is normalized against the number of starter neurons and averaged across animals. Data are mean ± s.e.m. ($n = 6$; $n = 3$). **o**, Schematic summary for input sources for PB_L-nociceptive neurons. BNST, bed nucleus of the stria terminalis; PVH, paraventricular hypothalamic nucleus; LHA, lateral hypothalamus; CeA_m, central amygdalar nucleus, medial; SN_{pc}, substantia nigra pars compacta; PAG, periaqueductal gray; DRn, dorsal raphe nucleus; DRn_{vl}, ventrolateral DRn; NST, nucleus of the solitary tract; Sp5C, trigeminal nucleus, caudalis; Pr5, principal sensory trigeminal nucleus; TG, trigeminal ganglion; DRG, dorsal root ganglion; S.C., spinal cord (dorsal horn). Reticular (ret.) nuclei: PRn, pontine reticular nuclei; IRt, intermediate reticular tract; PCRt, parvicellular reticular tract; MRn, medullary reticular nuclei; GRn, gigantocellular reticular nuclei. **p**, Molecular characterization of trans-synaptically labeled TG neurons. Green, bottom to top: IB4$^+$, CGRP$^+$, NF200$^+$, TrpV1$^+$. Left, colocalized trans-synaptically labeled TG neurons. Right, non-colocalized labeled TG neurons. Scale bars, 20 µm. **q**, Percentage of trans-synaptically labeled trigeminal ganglion neurons expressing IB4, CGRP, NF200, or TrpV1 ($n = 8$; one-way ANOVA; $^*P = 0.0135$, $^{***}P = 0.0008$, $^*P = 0.0468$, $^{****}P \leq 0.0001$, $^{****}P \leq 0.0001$, $P = 0.4653$; $F_{3,27} = 22.7$). Data are mean ± s.e.m. **r**, Schematic illustration and timeline of intraperitoneal injection in 1–2-day-old TrpV1-Cre pup with AAV9-CAG-flex-GFP. Four weeks after injection, TrpV1Cre::GFP mouse was injected with capsaicin in the whisker pad and sections stained for Fos ($n = 4$ mice). **s**, Representative image of trigeminal ganglion with TrpV1Cre::GFP$^+$ neurons. Scale bar, 200 µm. **t**, Representative image of PB_L with TrpV1Cre::GFP$^+$ axon terminals (green) and capsaicin-induced Fos$^+$ neurons (magenta). Scale bar, 50 µm (high magnification).

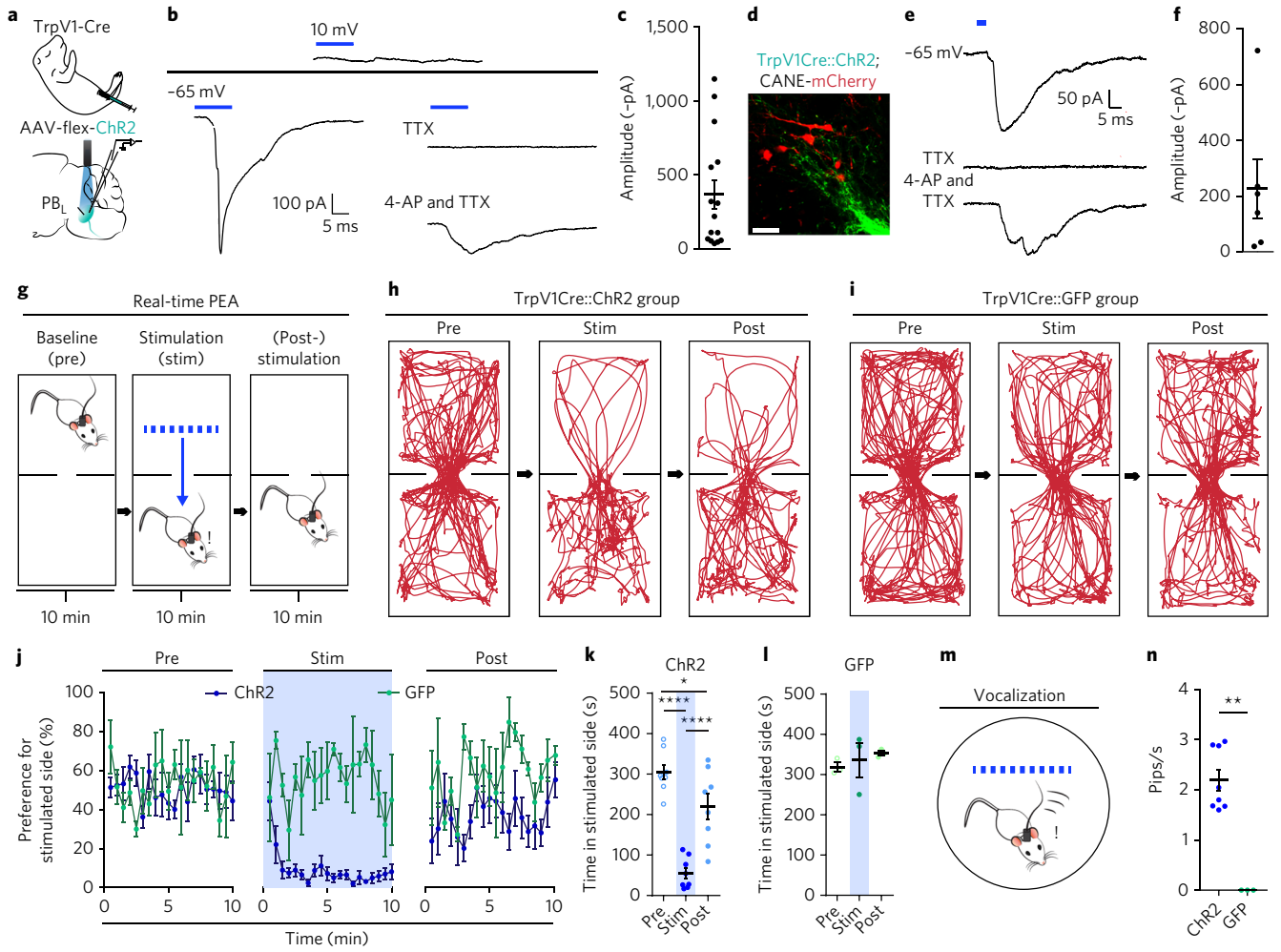

Fig. 4 | Optogenetic activation of TrpV1-Cre$^+$ sensory axons activates PB$_L$-nociceptive neurons and elicits aversive behavior and stress calls in a real-time place escape/avoidance task. a, Schematic illustration of intraperitoneal injection of a 1–2-day-old TrpV1-Cre pup ($n=3$), followed by optogenetic-assisted whole-cell patch-clamp recording from a PB$_L$ neuron in acute brain slices. **b**, Representative traces from a cell showing no light-evoked IPSC at a holding potential of 10 mV, but observed to have light-evoked EPSC at a holding of −65 mV. Cell, held at −65 mV, was bath applied 1 μM TTX, followed by 100 μM 4-AP and 1 μM TTX, and showed a light-evoked monosynaptic EPSC. **c**, Averaged current amplitude. Data are mean ± s.e.m. (closed circles represent individual cells, $n=15$). **d**, Representative high-magnification image of TrpV1Cre::ChR2$^+$ axon terminals and CANE-RV-mCherry captured PB$_L$-pain neurons ($n=3$ mice; scale bar, 50 μm). **e**, Representative example of an mCherry$^+$ PB$_L$-pain neuron recorded to have light-evoked EPSC at a holding of −65 mV. Cell was bath applied 1 μM TTX, followed by 100 μM 4-AP and 1 μM TTX, and showed a light-evoked monosynaptic EPSC. **f**, Averaged current amplitude. Data are mean ± s.e.m. (closed circles represent individual cells, $n=6$). **g**, Schematic illustration of real-time place escape/avoidance (PEA) test. **h**,**i**, Representative spatial tracking maps showing the location of (**h**) an experimental mouse before, during, and after optogenetic stimulation of TrpV1Cre::ChR2$^+$ axon terminals and (**h**) a control mouse before, during, and after illumination of TrpV1Cre::GFP$^+$ axon terminals in the PB$_L$ in the preferred chamber. **j**, Percentage of preference (per 30 s) the experimental and control groups had before, during, and after optogenetic stimulation ($n=8$, 3) shown across time (min). Data are mean ± s.e.m. **k**, Quantification of time the TrpV1Cre::ChR2 group spent in preferred chamber before, during, and after optogenetic stimulation ($n=8$ one-way repeated measures ANOVA; ****$P\leq0.0001$, *$P=0.0128$, ****$P\leq0.0001$; $F_{2,14}=49.41$). Data are mean ± s.e.m. **l**, Quantification of time the TrpV1Cre::GFP group spent in preferred chamber before, during, and after light illumination ($n=3$; one-way repeated measures ANOVA; $P=0.8867$, $P=0.6377$, $P=0.8886$; $F_{2,6}=0.4412$). Data are mean ± s.e.m. **m**, Schematic illustration of vocalization recording chamber. **n**, Quantification of frequency of pips induced by optogenetic stimulation of TrpV1Cre::ChR2 (experimental) or TrpV1Cre::GFP (control) axon terminals in the PB$_L$. Data are mean ± s.e.m. (ChR2, $n=8$; GFP, $n=3$; two-tailed unpaired Student's t test; **$P=<0.0001$; $t_7=10.13$).

PB in TrpV1-Cre; Ai65 mice (Supplementary Fig. 5a). Retrograde-lentivirus infects axons and is transported back to cell bodies[36,37]. Ai65 is a Cre and Flp co-dependent tomato reporter[38]. In this strategy, only TrpV1-Cre expressing neurons that project axons into PB will express both Cre and FlpO, and therefore only these neurons will express tomato, allowing us to visualize their cell bodies and axon projections. The Cre-dependent RG-LV-hSyn-DIO-FlpO gave sparser labeling results than the RG-LV-hSyn-FlpO. We observed tdTomato$^+$ neurons in ipsilateral TG (Supplementary Fig. 5c,f) but not in any DRG (data not shown). Interestingly, tdTomato$^+$ axons can be seen in both PB$_L$ and in Sp5C (Supplementary Fig. 5b,d,e,g), indicating that at least some of the labeled TG neurons project bifurcated axons to innervate both PB$_L$ and Sp5C. The peripheral axons of labeled TrpV1-Cre$^+$ TG→PB$_L$ neurons form either free nerve endings or circular endings around hair follicles (Supplementary Fig. 5h).

TrpV1-Cre$^+$ trigeminal sensory neurons provide monosynaptic excitatory input onto PB$_L$-pain neurons. To directly examine

whether TG→PB_L axons form functional synaptic connections in PB_L, we injected Cre-dependent AAV9-flex-ChR2-YFP into TrpV1-Cre pups intraperitoneally to express channelrhodospin-YFP (ChR2-YFP) in peripheral TrpV1-Cre$^+$ neurons (TrpV1Cre::ChR2) and performed whole-cell patch-clamp recording of PB_L neurons in slices from these animals (Fig. 4a). Photoactivation of

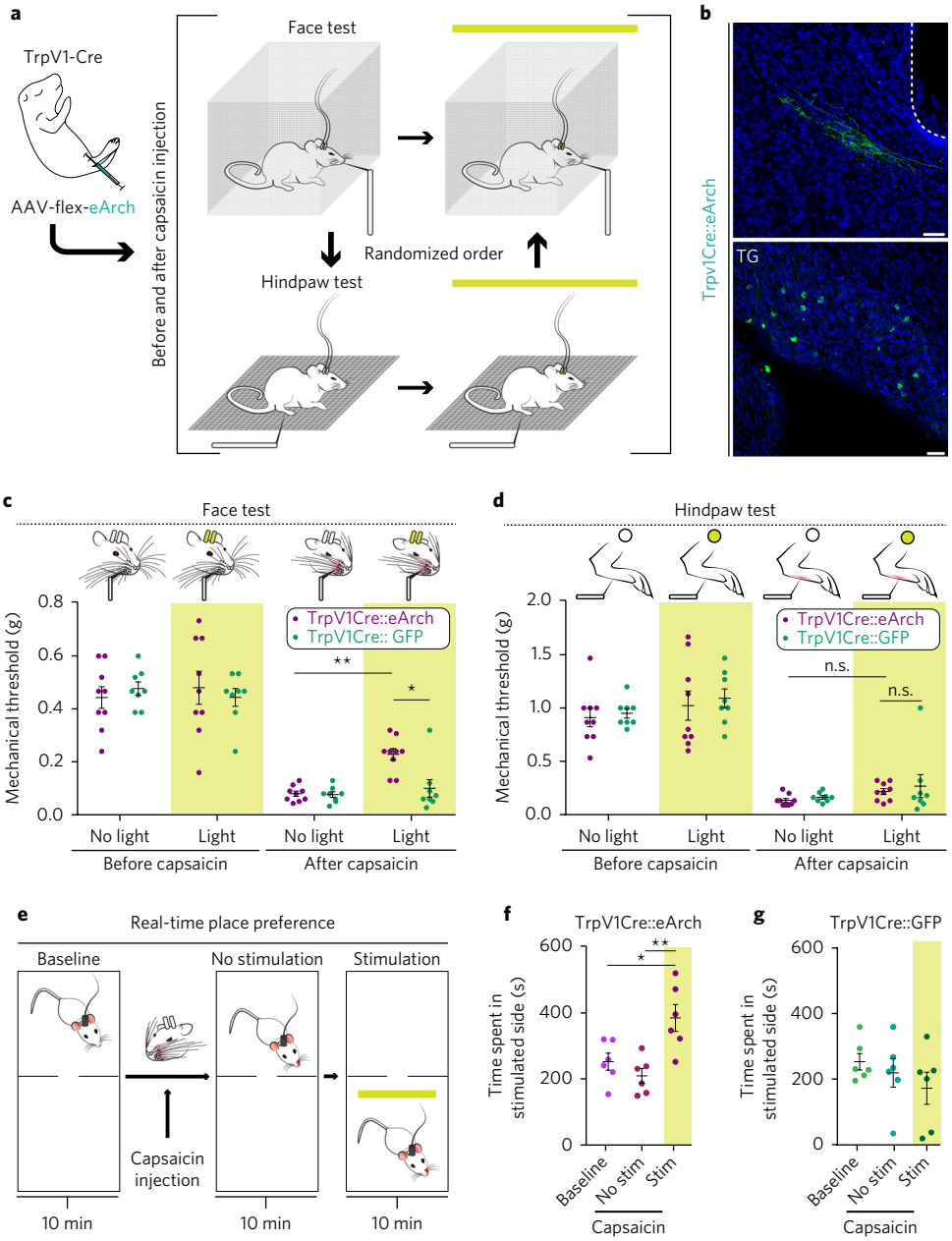

Fig. 5 | Optogenetic silencing of TrpV1-Cre$^+$ axon terminals in PB_L selectively reduces face allodynia after capsaicin injection. a, Schematic illustration of intraperitoneal injection of a 1–2-day-old TrpV1-Cre pup followed by face and hindpaw von Frey tests in the same individual mice in TrpV1Cre::eArch ($n=9$) and TrpV1Cre::GFP groups ($n=8$). The order of face versus hindpaw tests was randomized. Each mouse was tested before and after the injection of 10 µL 4% capsaicin into either face or hindpaw. **b**, Representative post-hoc image of TrpV1Cre::eArch$^+$ axon terminals in PB_L and labeled TrpV1Cre::eArch$^+$ cell bodies in TG ($n=9$ mice; scale bars, 50 µm). **c**, Quantification of mechanical thresholds of face withdrawal responses in von Frey tests. Measurements were taken before and after capsaicin injection into right whisker pad, as well as without and with optogenetic silencing, in TrpV1Cre::eArch ($n=9$) or in control TrpV1Cre::GFP groups ($n=8$, two-way repeated measures ANOVA; (eArch vs. GFP) $P\geq0.9999$, $P\geq0.9999$, $P\geq0.9999$, $^*P=0.0440$; (no light vs. light) eArch: $P\geq0.9999$, $^{**}P=0.0046$, GFP: $P\geq0.9999$, $P\geq0.9999$; $F_{3,45}=2.671$). Data are mean ± s.e.m. **d**, Quantification of mechanical thresholds of hindpaw withdrawal responses in von Frey tests. Measurements were taken before and after capsaicin injection into right hindpaw, as well as without and with optogenetic silencing in TrpV1Cre::eArch ($n=9$) or in TrpV1Cre::GFP groups ($n=8$, two-way repeated measures ANOVA; (Arch vs. GFP) $P\geq0.9999$, $P\geq0.9999$, $P\geq0.9999$, $P\geq0.9999$; (no light vs light) Arch: $P\geq0.9999$, $P\geq0.9999$, GFP: $P\geq0.9999$, $P\geq0.9999$; $F_{3,45}=0.03048$). Data are mean ± s.e.m. **e**, Schematic illustration of real-time place preference (RTPP) test of mouse injected with capsaicin into left whisker pad. **f**, Quantification of time the experimental group spent in non-preferred chamber before capsaicin, after capsaicin, and without or with optogenetic silencing ($n=6$ one-way repeated-measures ANOVA; $P=0.5356$, $^*P=0.0174$, $^{**}P=0.0031$; $F_{2,10}=10.92$). Data are mean ± s.e.m. **g**, Quantification of time the control group spent in non-preferred chamber before capsaicin, after capsaicin, and without or with optogenetic silencing ($n=7$; one-way repeated measures ANOVA; $P=0.7320$, $P=0.2086$, $P=0.5537$; $F_{2,10}=1.695$). Data are mean ± s.e.m.

TrpV1Cre::ChR2$^+$ terminals elicited excitatory post-synaptic currents (EPSCs) in 15 out of 54 neurons (Fig. 4b,c and Supplementary Fig. 6). Furthermore, the EPSCs persisted in the presence of action potential blockade caused by administration of 1 μM tetrodotoxin (TTX) and 100 μM 4-aminopyridine (4-AP) (Fig. 4b). In a complementary set of experiments, we captured PB_L-pain neurons using CANE-RV-mCherry in TrpV1Cre::ChR2 animals (Fig. 4d). In six CANE-captured mCherry$^+$ PB_L-pain neurons, photoactivation of TrpV1$^+$ terminals elicited EPSCs that were not blocked by TTX (Fig. 4e,f). These results corroborate and extend the circuit-tracing findings that the inputs from TG TrpV1-Cre$^+$ fibers to PB_L-nociceptive neurons are monosynaptic and excitatory.

Activation of TrpV1-Cre$^+$ axon terminals in PB_L induces robust aversive behavior and audible vocalization. To address the behavioral impact of the direct TG→PB_L monosynaptic projection in awake behaving animals, we asked whether its activation would be sufficient to elicit aversive responses in a modified real-time place escape/avoidance (PEA) assay, which has been used in recent studies to assay affective components of pain[39–41]. Optic fibers were implanted bilaterally above PB-el in either TrpV1Cre::ChR2 mice ($n=8$) or control mice TrpV1Cre::GFP ($n=3$) (Fig. 4g). Mice were habituated and placed in a two-chamber arena. Their behaviors were recorded under three conditions: (i) freely exploring with no stimulation for 10 min (baseline), followed by (ii) 10 min of conditioned photoactivation when the mouse is in its preferred chamber (stimulation), and followed again by (iii) 10 min without stimulation (post-stimulation). Upon photo-stimulation of TrpV1Cre$^+$ axons in PB-el, TrpV1Cre::ChR2 mice immediately fled to the opposite chamber (Fig. 4h; Supplementary Video 1), and subsequently they moved less and spent significantly more time on the unstimulated side (Fig. 4h,j,k, Supplementary Video 1; $P<0.0001$). In the post-stimulation period, some but not all mice still showed avoidance of the chamber in which they received photostimulation (Fig. 4j,k). Light illumination had no effect on movement and behavior of the control TrpV1Cre::GFP mice (Fig. 4i,j,l, Supplementary Video 2; $P=0.66$). These results suggest that the optogenetic stimulation of the TG→PB_L monosynaptic projection caused a drastic aversive effect that is likely to be due to activation of the downstream affective pain pathway.

We further wanted to determine whether optogenetic activation would be sufficient to induce an aversive affective memory using the conventional conditioned place aversion (CPA) assay (Supplementary Fig. 7a). Mice were habituated first by placing them in the two-chamber arena and allowing free exploration. Subsequently, they were subjected to 2 d of conditioning: mice were paired with photostimulation in the preferred chamber for 15 min, and 4 h later they were placed in the non-preferred chamber with no stimulation for 15 min. On the fourth day, they explored the arena freely with no light stimulation for 10 min (post-stimulation). All TrpV1Cre::ChR2 mice ($n=7$) spent less time in the chamber where they were stimulated previously (Supplementary Fig. 7b,c; $P=0.008$). Light illumination had no effect on the movement and behavior of the control TrpV1Cre::GFP mice ($n=5$; Supplementary Fig. 7d,e; $P=0.258$). These results suggest that repeated optogenetic activation of the TG→PB_L monosynaptic projection induces an aversive memory.

We further recorded audios of mice placed in a circular arena (Fig. 4m). Optogenetic activation of TrpV1-Cre$^+$ afferents in PB-el induced audible vocalizations in TrpV1Cre::ChR2 mice ($n=8$) resembling distress calls, but not in control TrpV1Cre::GFP mice ($n=3$) (Fig. 4n; Supplementary Fig. 8, Supplementary Videos 3 and 4; on average 66 ± 7 pips with 2 ± 0.2 pips/second were elicited; $P<0.0001$). Distress vocalization stopped when laser light was turned off. Post-hoc immunostaining conducted after photostimulation of the TrpV1Cre::ChR2 axon terminals in the PB_L showed marked Fos expression in this region, whereas only background Fos expression was observed in Sp5C (Supplementary Fig. 9a,b), indicating that there was little back-propagation of activities from PB_L axon-terminal photostimulation to the axon branches of TG sensory neurons in Sp5C. Post-hoc immunostaining after photostimulation of TrpV1Cre::GFP axon terminals only showed background-level Fos expression (Supplementary Fig. 9c; $n=5$). Taken together, these data demonstrate that activating the direct axonal projection from TrpV1-Cre$^+$ terminals in PB-el is sufficient to induce robust escape/avoidance behavior, aversive memory, and audible distress vocalizations, which are surrogates of pain behavior and pain-associated negative affect.

Silencing TrpV1-Cre$^+$ axon terminals in PB_L selectively reduces facial allodynia after capsaicin injection. We next asked whether silencing the direct TG→PB_L monosynaptic projection would affect pain-related behaviors. Previous studies showed that the optogenetic silencer archaerhodopsin (Arch) can effectively silence nociceptors including TrpV1 + neurons[42,43]. We therefore used the neonatal IP injection strategy to express eArch[44] or GFP in TrpV1-Cre$^+$ sensory neurons. Optic fibers were implanted bilaterally above PB-el in TrpV1Cre::eArch mice ($n=9$) or TrpV1Cre::GFP ($n=8$) mice (Fig. 5a,b). A von Frey test was used to assess the mechanical threshold of face or paw withdrawal responses before and after capsaicin injections into the whisker pad or hindpaw and with or without photosilencing of TrpV1-Cre$^+$ axons in PB_L (Fig. 5a). After capsaicin injection into either the face or the paw, both TrpV1Cre::eArch and TrpV1Cre::GFP mice drastically lowered the withdrawal threshold in responses to von Frey application to face or paw, respectively (Fig. 5c,d). Hence, capsaicin injection induced mechanical allodynia in both face and hindpaw as expected (Fig. 5c,d). Importantly, eArch-mediated photosilencing of TrpV1-Cre$^+$ axons in PB-el partially alleviated the capsaicin induced allodynia in the face but had no effect on the mechanical hypersensitivity of the hindpaw (Fig. 5c,d; face $P=0.0046$, paw $P\geq0.9999$). Light illumination had no effect on TrpV1Cre::GFP mice (Fig. 5c,d; $P\geq0.9999$). These results confirmed that the TG→PB_L direct pathway indeed specifically contributes to face nociception.

We further tested whether photosilencing of TrpV1-Cre$^+$ axons in PB_L after facial capsaicin injection would elicit conditioned place preference for the light illuminated chamber. The effect of capsaicin only lasts about 20 min, and we therefore performed a real-time place preference (RTPP) assay (Fig. 5e; 10 min without light and 10 min with light illumination in the non-preferred chamber). After capsaicin injection into the whisker pad, TrpV1Cre::eArch mice spent significantly more time in the chamber with photosilencing of the TrpV1-Cre$^+$ terminals in PB_L (Fig. 5f; $n=6$; $P=0.029$). By contrast, control TrpV1Cre::GFP mice show no preference (Fig. 5g; $n=7$; $P=0.6$). Taken together, these data demonstrated that when mice are subjected to noxious facial stimulation, silencing the neural activity of the direct TG→PB_L pathway reduces facial allodynia and induces place preference, indicating that this pathway contributes significantly to the manifestation of facial-pain equivalents.

Discussion

In this study, we discovered that nociceptive trigeminal afferents transmit painful signal to the affective pathway through both the direct monosynaptic TG→PB_L and the indirect disynaptic TG→Sp5C→PB_L projections. In a previous study, researchers injected neural tracer WGA-HRP into the peripheral anterior ethmoidal nerve (AEN), which originates from TG and innervates the nasal cavity, and observed labeled afferent fibers in regions near PB_L[31]. In a follow-up study, the authors showed that trigeminal rhizotomy results in loss of CGRP-expressing fibers innervating the PB_L[30].

These and other studies have implied that a direct TG→PB_L pathway might exist[29–32] but have not provided synaptic or behavior evidence to support this possibility. Here we used a combination of activity-dependent tagging, monosynaptic trans-synaptic tracing, intersectional genetic labeling, optogenetic-assisted slice electrophysiology, and in vivo optogenetic activation and silencing experiments to definitely establish the monosynaptic connection between TG and PB_L-nociceptive neurons, and revealed the important functions of this pathway in craniofacial-pain-related aversive behaviors.

Our findings have several important implications. First, the dual and bilateral pain-transmitting pathways compared to the single indirect DRG→dorsal horn→PB_L pathway could explain why similar-intensity stimuli applied to face activate more PB_L neurons than when applied to limbs. This could in turn lead to heightened and bilateral activations of the affective pain responses, such as a higher level and more persistent activation of CeA, BNST, hypothalamus and insular cortex through the axonal projections from PB_L-nociceptive neurons (Fig. 2k–r). This projection pattern can provide a circuit basis for the perception of trigeminally mediated pain as more severe, fear inducing and emotionally draining than other body pain. The monosynaptic TG→PB_L connection also provides a mechanism for rapid, short-latency direct connections of nociceptive inputs from the head and face to brain centers involved in homeostatic regulation and emotional processing[5,6,15,21,23,45]. Second, current palliative neurosurgical procedures aimed at alleviating refractory trigeminal pain target the descending spinal trigeminal tract (Supplementary Fig. 10), including making thermal lesions, referred to as 'dorsal root entry zone coagulation' (DREZ), to lesion-pain-transmitting pathways in Sp5C, a contemporary adaptation of the classic trigeminal tractotomy[46,47]. Based on our study, DREZ coagulation will lesion only the TG→Sp5C connection, while leaving the TG→PB_L connection intact (Supplementary Fig. 10). This may explain the lack of therapeutic response or postoperative pain relapse seen in some patients subjected to trigeminal DREZ surgery[46–48]. Designers of future surgical procedures should consider severing both the TG→Sp5C and TG→PB_L connections as a means to provide invasive palliation of chronic, refractory orofacial pain, for example, for trigeminal neuralgia. Notably, our discovery presented here critically relied on the CANE methodology, although CANE does have qualifiers, namely that the 60–90-min waiting interval between the stimulus application and the surgery (in order for Fos^{TVA} protein to reach peak levels) inevitably resulted in some background labeling. Nevertheless, CANE is still the best-validated tool to selectively label and trans-synaptically trace the presynaptic inputs to transiently activated neurons as shown here and in our previous studies[12]. Our input–output circuit mapping of PB_L-nociceptive neurons revealed many limbic centers that are reciprocally connected with PB_L, providing a circuit basis for understanding comorbidities that are closely associated with and clinically highly relevant to pathologic trigeminal pain, namely anxiety, depression, disturbance of circadian rhythm and altered intake behavior[2,3,47–50]. Future studies on mechanisms underlying chronic craniofacial pain disorders can now take advantage of this circuit diagram including the newly unveiled monosynaptic TG→PB_L pathway to identify specific maladaptive plasticity in each of the nodes in the circuit and, it can be hoped, to effectively revert them.

Methods

Methods, including statements of data availability and any associated accession codes and references, are available at https://doi.org/10.1038/s41593-017-0012-1.

Received: 9 August 2017; Accepted: 22 September 2017;
Published online: 13 November 2017

References

1. Waldman, S. D. *Atlas of Common Pain Syndromes* (Elsevier Health Sciences, Philadelphia, 2011).
2. Zakrzewska, J. M., Wu, J., Mon-Williams, M., Phillips, N. & Pavitt, S. H. Evaluating the impact of trigeminal neuralgia. *Pain* **158**, 1166–1174 (2017).
3. Smith, J. G. et al. The psychosocial and affective burden of posttraumatic neuropathy following injuries to the trigeminal nerve. *J. Orofac. Pain* **27**, 293–303 (2013).
4. Schmidt, K., Schunke, O., Forkmann, K. & Bingel, U. Enhanced short-term sensitization of facial compared with limb heat pain. *J. Pain* **16**, 781–790 (2015).
5. Schmidt, K. et al. The differential effect of trigeminal vs. peripheral pain stimulation on visual processing and memory encoding is influenced by pain-related fear. *Neuroimage* **134**, 386–395 (2016).
6. Moulton, E. A. et al. Capsaicin-induced thermal hyperalgesia and sensitization in the human trigeminal nociceptive pathway: an fMRI study. *Neuroimage* **35**, 1586–1600 (2007).
7. Hunt, S. P. & Mantyh, P. W. The molecular dynamics of pain control. *Nat. Rev. Neurosci.* **2**, 83–91 (2001).
8. Gauriau, C. & Bernard, J.-F. F. Pain pathways and parabrachial circuits in the rat. *Exp. Physiol* **87**, 251–258 (2002).
9. Craig, A. D. Distribution of brainstem projections from spinal lamina I neurons in the cat and the monkey. *J. Comp. Neurol.* **361**, 225–248 (1995).
10. Hermanson, O. & Blomqvist, A. Subnuclear localization of FOS-like immunoreactivity in the rat parabrachial nucleus after nociceptive stimulation. *J. Comp. Neurol.* **368**, 45–56 (1996).
11. Hermanson, O. & Blomqvist, A. Subnuclear localization of FOS-like immunoreactivity in the parabrachial nucleus after orofacial nociceptive stimulation of the awake rat. *J. Comp. Neurol.* **387**, 114–123 (1997).
12. Sakurai, K. et al. Capturing and manipulating activated neuronal ensembles with CANE delineates a hypothalamic social-fear circuit. *Neuron* **92**, 739–753 (2016).
13. Slugg, R. M. & Light, A. R. Spinal cord and trigeminal projections to the pontine parabrachial region in the rat as demonstrated with *Phaseolus vulgaris* leucoagglutinin. *J. Comp. Neurol.* **339**, 49–61 (1994).
14. Cechetto, D. F., Standaert, D. G. & Saper, C. B. Spinal and trigeminal dorsal horn projections to the parabrachial nucleus in the rat. *J. Comp. Neurol.* **240**, 153–160 (1985).
15. Han, S., Soleiman, M. T., Soden, M. E., Zweifel, L. S. & Palmiter, R. D. Elucidating an affective pain circuit that creates a threat memory. *Cell* **162**, 363–374 (2015).
16. Gaub, S., Fisher, S. E. & Ehret, G. Ultrasonic vocalizations of adult male Foxp2-mutant mice: behavioral contexts of arousal and emotion. *Genes Brain Behav* **15**, 243–259 (2016).
17. Geerling, J. C. et al. FoxP2 expression defines dorsolateral pontine neurons activated by sodium deprivation. *Brain Res.* **1375**, 19–27 (2011).
18. Ding, Y. Q., Takada, M., Shigemoto, R. & Mizuno, N. Trigeminoparabrachial projection neurons showing substance P receptor-like immunoreactivity in the rat. *Neurosci. Res.* **23**, 415–418 (1995).
19. Tokita, K., Inoue, T. & Boughter, J. D. Jr. Afferent connections of the parabrachial nucleus in C57BL/6J mice. *Neuroscience* **161**, 475–488 (2009).
20. Nishijo, H. & Norgren, R. Parabrachial neural coding of taste stimuli in awake rats. *J. Neurophysiol.* **78**, 2254–2268 (1997).
21. Nakamura, K. & Morrison, S. F. A thermosensory pathway that controls body temperature. *Nat. Neurosci.* **11**, 62–71 (2008).
22. Alhadeff, A. L., Golub, D., Hayes, M. R. & Grill, H. J. Peptide YY signaling in the lateral parabrachial nucleus increases food intake through the Y1 receptor. *Am. J. Physiol. Endocrinol. Metab.* **309**, E759–E766 (2015).
23. Davern, P. J. A role for the lateral parabrachial nucleus in cardiovascular function and fluid homeostasis. *Front. Physiol* **5**, 436 (2014).
24. Menani, J. V., De Luca, L. A. Jr. & Johnson, A. K. Role of the lateral parabrachial nucleus in the control of sodium appetite. *Am. J. Physiol. Regul. Integr. Comp. Physiol.* **306**, R201–R210 (2014).
25. Bester, H., Menendez, L., Besson, J. M. & Bernard, J. F. Spino (trigemino) parabrachiohypothalamic pathway: electrophysiological evidence for an involvement in pain processes. *J. Neurophysiol.* **73**, 568–585 (1995).
26. Bernard, J. F. & Besson, J. M. The spino(trigemino)pontoamygdaloid pathway: electrophysiological evidence for an involvement in pain processes. *J. Neurophysiol.* **63**, 473–490 (1990).
27. Oh, S. W. et al. A mesoscale connectome of the mouse brain. *Nature* **508**, 207–214 (2014).
28. Kohara, K. et al. Cell type–specific genetic and optogenetic tools reveal hippocampal CA2 circuits. *Nat. Neurosci.* **17**, 269–279 (2014).
29. Cavanaugh, D. J. et al. Restriction of transient receptor potential vanilloid-1 to the peptidergic subset of primary afferent neurons follows its developmental downregulation in nonpeptidergic neurons. *J. Neurosci.* **31**, 10119–10127 (2011).

30. Panneton, W. M. & Gan, Q. Direct reticular projections of trigeminal sensory fibers immunoreactive to CGRP: potential monosynaptic somatoautonomic projections. *Front. Neurosci.* **8**, 136 (2014).
31. Panneton, W. M., Gan, Q. & Juric, R. Brainstem projections from recipient zones of the anterior ethmoidal nerve in the medullary dorsal horn. *Neuroscience* **141**, 889–906 (2006).
32. Cavanaugh, D. J. et al. Trpv1 reporter mice reveal highly restricted brain distribution and functional expression in arteriolar smooth muscle cells. *J. Neurosci.* **31**, 5067–5077 (2011).
33. Mishra, S. K., Tisel, S. M., Orestes, P., Bhangoo, S. K. & Hoon, M. A. TRPV1-lineage neurons are required for thermal sensation. *EMBO J* **30**, 582–593 (2011).
34. Foust, K. D., Poirier, A., Pacak, C. A., Mandel, R. J. & Flotte, T. R. Neonatal intraperitoneal or intravenous injections of recombinant adeno-associated virus type 8 transduce dorsal root ganglia and lower motor neurons. *Hum. Gene Ther.* **19**, 61–70 (2008).
35. Machida, A. et al. Intraperitoneal administration of AAV9-shRNA inhibits target gene expression in the dorsal root ganglia of neonatal mice. *Mol. Pain* **9**, 36 (2013).
36. Stanek, E. IV, Rodriguez, E., Zhao, S., Han, B.-X. X. & Wang, F. Supratrigeminal bilaterally projecting neurons maintain basal tone and enable bilateral phasic activation of jaw-closing muscles. *J. Neurosci.* **36**, 7663–7675 (2016).
37. Bellavance, M. A. et al. Parallel inhibitory and excitatory trigemino-facial feedback circuitry for reflexive vibrissa movement. *Neuron* **95**, 673–682.e4 (2017).
38. Madisen, L. et al. Transgenic mice for intersectional targeting of neural sensors and effectors with high specificity and performance. *Neuron* **85**, 942–958 (2015).
39. Baastrup, C., Jensen, T. S. & Finnerup, N. B. Pregabalin attenuates place escape/avoidance behavior in a rat model of spinal cord injury. *Brain Res.* **1370**, 129–135 (2011).
40. LaBuda, C. J. & Fuchs, P. N. A behavioral test paradigm to measure the aversive quality of inflammatory and neuropathic pain in rats. *Exp. Neurol.* **163**, 490–494 (2000).
41. Zhang, Z. et al. Role of prelimbic GABAergic circuits in sensory and emotional aspects of neuropathic pain. *Cell Rep.* **12**, 752–759 (2015).
42. Daou, I. et al. Optogenetic silencing of Nav1.8-positive afferents alleviates inflammatory and neuropathic pain. *eNeuro* **3**, 0140-15.2016 (2016).
43. Li, B. et al. A novel analgesic approach to optogenetically and specifically inhibit pain transmission using TRPV1 promoter. *Brain Res* **1609**, 12–20 (2015).
44. Chow, B. Y. et al. High-performance genetically targetable optical neural silencing by light-driven proton pumps. *Nature* **463**, 98–102 (2010).
45. Sato, M. et al. The lateral parabrachial nucleus is actively involved in the acquisition of fear memory in mice. *Mol. Brain* **8**, 22 (2015).
46. Moffie, D. Late results of bulbar trigeminal tractotomy. *Some remarks on recovery of sensibility. J. Neurol. Neurosurg. Psychiatry* **34**, 270–274 (1971).
47. Rahimpour, S. & Lad, S. P. Surgical options for atypical facial pain syndromes. *Neurosurg. Clin. N. Am.* **27**, 365–370 (2016).
48. Romaniello, A., Iannetti, G. D., Truini, A. & Cruccu, G. Trigeminal responses to laser stimuli. *Clin. Neurophysiol.* **33**, 315–324 (2003).
49. DeSouza, D. D., Moayedi, M., Chen, D. Q., Davis, K. D. & Hodaie, M. sensorimotor and pain modulation brain abnormalities in trigeminal neuralgia: a paroxysmal, sensory-triggered neuropathic pain. *PLoS One* **8**, e66340 (2013).
50. Kuner, R. Central mechanisms of pathological pain. *Nat. Med.* **16**, 1258–1266 (2010).
51. Zhang, F. et al. Optogenetic interrogation of neural circuits: technology for probing mammalian brain structures. *Nat. Protoc.* **5**, 439–456 (2010).
52. Röhn, T. A. et al. A virus-like particle-based anti-nerve growth factor vaccine reduces inflammatory hyperalgesia: potential long-term therapy for chronic pain. *J. Immunol.* **186**, 1769–1780 (2011).
53. Xu, Z. Z. et al. Inhibition of mechanical allodynia in neuropathic pain by TLR5-mediated A-fiber blockade. *Nat. Med.* **21**, 1326–1331 (2015).
54. Koh, W. U. et al. Perineural pretreatment of bee venom attenuated the development of allodynia in the spinal nerve ligation injured neuropathic pain model; an experimental study. *BMC Complement. Altern. Med.* **14**, 431 (2014).
55. Jennings, J. H. et al. Distinct extended amygdala circuits for divergent motivational states. *Nature* **496**, 224–228 (2013).
56. Stamatakis, A. M. & Stuber, G. D. Activation of lateral habenula inputs to the ventral midbrain promotes behavioral avoidance. *Nat. Neurosci.* **15**, 1105–1107 (2012).
57. Lopes, G. et al. Bonsai: an event-based framework for processing and controlling data streams. *Front. Neuroinform* **9**, 7 (2015).
58. Silva, J. R. et al. Neuroimmune-glia interactions in the sensory ganglia account for the development of acute herpetic neuralgia. *J. Neurosci.* **37**, 6408–6422 (2017).
59. Peng, C. et al. miR-183 cluster scales mechanical pain sensitivity by regulating basal and neuropathic pain genes. *Science* **356**, 1168–1171 (2017).
60. Kim, Y. S. et al. Central terminal sensitization of TRPV1 by descending serotonergic facilitation modulates chronic pain. *Neuron* **81**, 873–887 (2014).
61. Aita, M., Byers, M. R., Chavkin, C. & Xu, M. Trigeminal injury causes kappa opioid-dependent allodynic, glial and immune cell responses in mice. *Mol. Pain* **6**, 8 (2010).
62. Zhang, Y. et al. Identifying local and descending inputs for primary sensory neurons. *J. Clin. Invest* **125**, 3782–3794 (2015).
63. Zhang, Y., Chen, Y., Liedtke, W. & Wang, F. Lack of evidence for ectopic sprouting of genetically labeled Aβ touch afferents in inflammatory and neuropathic trigeminal pain. *Mol. Pain* **11**, 18 (2015).

Acknowledgements

We thank J. Takatoh for helping with a method to quantify axon innervation densities, K. Tschida and T. Gibson for helping with vocalization quantification and analysis, and V. Prevosto for helping with statistics. We also thank T. Gibson, M. Fu, K. Tschida, T. Stanek, V. Prevosto, and R. R. Ji for providing input and support throughout the project, and S. Lisberger and R. Mooney for critical reading of this manuscript. E.R. is supported by a F31 DE025197-03 fellowship. Y.C. is supported by K12DE022793. W.L. is supported by DE018549. This work is supported by NIH Grant DP1MH103908 to F.W.

Author contributions

F.W. and E.R. conceived the idea and designed the experiments. E.R. performed the majority of the experiments and data analysis. K.S. performed some independent CANE capture experiments, bilateral fiber implantations and the place escape/avoidance (PEA) behavioral experiments. K.T. analyzed PEA results (blind to genotype). J.X. performed immunohistochemistry, quantified axon projections, and quantified cells in Fos and trans-synaptic experiments (blind to experimental conditions). Y.C. performed all the face and hindpaw von Frey assays (blind to genotypes). D.R. quantified cells in a subset of colocalization experiments. S.Z. produced all the CANE-LV and CANE-RV viruses. B.-X.H. took care of mouse husbandry and genotyping. H.Y. and W.L. provided critical equipment and reagents. F.W. and E.R. wrote the manuscript with help from W.L.

Competing interests

The authors declare no competing financial interests.

Additional information

Supplementary information is available for this paper at https://doi.org/10.1038/s41593-017-0012-1.

Reprints and permissions information is available at www.nature.com/reprints.

Correspondence and requests for materials should be addressed to F.W.

Publisher's note: Springer Nature remains neutral with regard to jurisdictional claims in published maps and institutional affiliations.

Methods

Animal statement. All experiments were conducted according to protocols approved by The Duke University Institutional Animal Care and Use Committee.

Animals. Adult (P30-P60) male and female C57B/L6 mice (Jackson Laboratory) were used for immunohistochemistry and in situ hybridization. Male and female Fos^{TVA} mice[12] (Jackson Laboratory, stock 027831) were used for capturing PB_L-nociceptive neurons with the CANE technology, immunohistochemistry, electrophysiology, and input-output circuit mapping. Male and female Ai65D[38] mice expressing a Cre and Flp double-dependent STOP cassette in front of the tdTomato reporter (Jackson Laboratories, stock 024109) were used for Cre/FlpO based tracing of $TrpV1Cre^+$ neurons that project to PB_L. Male and female TrpV1-Cre mice[33] were used for behavioral testing for both ChR2 or eArch experimental and GFP control groups, as well as electrophysiology experiments. Male and female Ai32 mice expressing a Cre-dependent ChR2 (Jackson Laboratories, stock 024109) were used for electrophysiology experiments. All mice were housed in a vivarium with normal light/dark cycles in cages with 1–5 mice. A day before experiments, we singly housed mice. We used two exclusion criteria for our subjects: (1) poor recovery or other health concerns following surgical intervention or (2) missed injection or implantation target, as determined by histological analysis. Animals were randomly selected from each litter. Random group allocation was maintained throughout the study, within constraints set by availability of in-house, purpose-bred lines. Experimenter blinding was sufficient to control for selection bias. Furthermore, behavioral analysis relied on objective, automatized measurements.

Viruses. CANE-LV-Cre (titer, 5×10^8 ifu/ml; pLenti-hSynapsin-Cre-WPRE [Addgene Plasmid #86641]; CANE-LV envelope [Addgene Plasmid #86666]) and CANE-RV-mCherry (titer, 5×10^8 ifu/ml) were produced as previously described[12]. FuGB2-coated RG-LV-hSyn-FlpO and RG-LV-hSyn-DIO-FlpO were produced and concentrated as described previously[36]. pAAV-SynP-DIO-TVA-EGFP-RG (pAAV-SynP-DIO-sTpEpB)[28] was packaged in serotype AAV2/rh8 by the University of Pennsylvania Vector Core. AAV-CAG-flex-GFP, AAV-EF1α-flex-ChR2(H134R)-eYFP[51] and AAV-EF1α-DIO-eARCH-eYFP[44] were purchased from the University of Pennsylvania Vector Core.

Surgery. Animals were anesthetized with isoflurane in a stereotaxic frame (David Kopf Instruments) and small craniotomies were made over the target area. To target the PB_L, mice were mounted in the stereotaxic frame at an angle such that lambda was ~180 µm ventral to bregma (in practice, 140–240 µm). The stereotaxic coordinates of virus injection and custom-made optic fiber (200 µm core diameter, Thorlabs) were AP − 4.25 ± 0.15 mm, ML 1.45 ± 0.15 mm, and DV −3.2 ± 0.1 mm. The thin glass capillary was slowly lowered to the target site to minimize the brain injury. Virus was delivered into the target site at a flow rate of 100 nl per min using a pulled thin glass capillary (Warner Instruments) connected to an UltraMicroPump controlled by a SYS-Micro4 Controller 15 (World Precision Instruments).

For transsynaptic labeling experiment, CANE-LV-Cre and AAV-SynP-DIO-TVA-EGFP-RG were co-injected in animals subjected to 4% formalin injection; injected animals were singly housed for 2 weeks followed by CANE-RV-mCherry injection. For retrograde labeling experiment, RG-LV-hSyn-FlpO or RG-LV-hSyn-DIO-FlpO were injected in TrpV1Cre::Ai65D animals.

For neonatal intraperitoneal (IP) injections, postnatal day 1–2 pups were anesthetized with hyperthermia. 6 weeks after neonatal IP injection, mice were subjected to bilateral implantation of a custom-made optic fiber. After another 1–2 weeks of recovery, implanted animals were subjected to behavioral testing.

The injected viruses and the waiting period for viral transgene expression for the different experiments are: for experiments in Fig. 2, CANE-LV-Cre (500 nl) together with AAV-CAG-flex-GFP (300 nl), waiting > 10 days or > 4 weeks; for experiments in Fig. 3a–o, CANE-LV-Cre (500 nl) together with AAV-SynP-DIO-TVA-EGFP-RG (200 nl), waiting 2 weeks, then CANE-RV-mCherry (1:200 dilution, 300 nl), waiting additional 10 days; for experiment in Fig. 4d–f, CANE-RV-mCherry (1:200 dilution, 300 nl), waiting 3 days. For experiments in Figs. 3r–t and 4a–c,g–m, AAV9-CAG-flex-GFP (5 µL) or AAV9-EF1α-DIO-hChR2-eYFP (5 µL), waiting 4–6 weeks. For experiments in Fig. 5, AAV9-EF1α -DIO-eArch-eYFP (8 µL), waiting 4–6 weeks. For experiments in Supplementary Fig. 5, RG-LV-h-Syn-DIO-FlpO or RG-LV-hSyn-FlpO (800 nL), waiting 3 weeks.

Immunohistochemistry. All mice were deeply anaesthetized with isoflurane, and then transcardially perfused with ice-cold 4% paraformaldehyde in 0.1 M phosphate buffer, pH 7.4 (4% PFA). Dissected brain samples were then post-fixed overnight in 4% PFA at 4 °C, cryoprotected in a 20% sucrose solution in PBS at 4 °C, frozen in Tissue-Tek O.C.T. Compound (Sakura) and stored at −80 °C until sectioning. Trigeminal and dorsal root ganglion samples were sliced at 20 µm using a cryostat (Leica Biosystems). All other coronal brain sections were sliced at 60–80 µm. The serial brain sections were collected in a 24 well plate and washed with PBS 3 times. The sections were blocked with 2% bovine serum albumin (BSA) in PBS with 0.3% Triton X-100 (blocking solution) at room temperature for 1 h. The sections were treated with primary antibody in blocking solution at 4 °C for overnight. The sections were washed 3 times followed by secondary antibody treatment at 4 °C for 2 h. Sections were counter-stained NeuroTrace fluorescent Nissl stain (fluorescent Nissl stain) (Invitrogen, N-21479) or 4′,6-diamidino-2-phenylindole (DAPI) (Sigma, D9564). After this incubation, sections were washed, mounted and coverslipped. The primary antibodies used in this study are: goat anti-Fos[12] (Santa Cruz Biotechnology, sc52-g, 1:300), rabbit anti-CGRP[52] (Millipore, AB15360, 1:1,000), sheep anti-FoxP2[17] (R&D Systems, AF5647, 1:5,000), rabbit anti-NF200[53] (Sigma, N4142, 1:200), GS-IB4-Alexa 488–conjugated (Invitrogen, I21411, 1:1,000), rabbit anti-VR1(TrpV1)[54] (Abcam, ab31895, 1:1,000), and rabbit anti-GFP[12] (Abcam, ab290, 1:1,000). The secondary antibodies are: Alexa Fluor 488 donkey anti-goat (Jackson Immunoresearch, 705-545-147 1:1,000), Cy3 donkey anti-goat (Jackson Immunoresearch, 705-165-147, 1:1,000), Alexa Fluor 488 donkey anti-rabbit (Jackson Immunoresearch, 703-545-155, 1:1,000), Cy3 donkey anti-rabbit (Jackson Immunoresearch, 711-165-152, 1:1,000), and Alexa Fluor 488 donkey anti-sheep (Abcam, ab150181, 1:1,000)

Floating section in situ hybridization. For each mouse, six 60 µm sections containing the PB_L were collected and in situ was performed as described previously[36]. *Gad1*, *Gad2*, *vGlut2* and *Fos* probes were created as previously described[12,37], and *Gad1* and *Gad2* probes were applied as a mixed probe. The probes were alternated across all sections to ensure that one posterior section and one anterior section from each region was analyzed with each probe type.

Image acquisition and quantification. Samples were imaged using a Zeiss 700 laser scanning confocal microscope. In situ samples were imaged at 20× resolution at three *z*-positions. All *z*-positions for each slice were merged into a single image in Adobe Photoshop CS6 for quantification. All other samples were imaged at 10× resolution. The captured neurons and Fos expressing neurons in all immunohistochemistry and in situ hybridization experiments were manually counted, and percentages were calculated within each animal before averaging percentages across animals.

Axonal projections from captured PB_L-nociceptive neurons was quantified using a method previously described[12,28]. The projection density for ROI's was quantified across every other 80 µm coronal section. The data was normalized between animals by their own values in CeA (central amygdala). ROIs with densities in which the total pixel numbers of GFP-labeled axons divided by the area of the nuclei was less than 0.1 were excluded.

Again, using a method previously described[12], the number of transsynaptically labeled neurons from captured PB_L-nociceptive neurons was quantified across every other 80 µm coronal section. Numbers of labeled cells in each ROI were manually counted. The data was normalized between animals by dividing with the number of starter neurons (GFP and mCherry double positive neurons in the PB_L) in each animal.

Behavioral experiments for Fos immunostaining. Adult male and female C57B/L6 mice at ages more than 6 weeks were singly housed at least one day before noxious stimulation. Singly housed mice were directly perfused to stain for background Fos expression. For visualizing Fos expression induced by nociceptive stimuli, mice were lightly anesthetized with isoflurane and unilaterally injected with 10 µl of saline, or 4% capsaicin, or 4% formalin into either the whisker pad or the hindpaw and returned to their home cage. 90 min later, the animals were perfused (as described in the method for immunostaining above).

Behavioral experiments for capturing PB_L-nociceptive neurons with CANE virus. A brief description of CANE method: in Fos^{TVA} mice, activated neurons transiently express Fos which induces expression of a destabilized TVA (dsTVA) receptor. Lentivirus or deficient rabies virus pseudotyped with an engineered mutated envelope protein (CANE envelope) specifically binds cells expressing high-level TVA receptor, which are strongly Fos^+ neurons. In this way, CANE-viruses selectively infect Fos^+ neurons and deliver desired transgenes to be expressed in Fos^+ neurons.

Here, adult male and female Fos^{TVA} mice at ages more than 6 weeks were singly housed for at least one day, and then either handled without injection, or handled and subjected to noxious stimulation. Briefly, mice were taken out of their home cage, placed in the anesthesia chamber, lightly anesthetized with isoflurane, and injected unilaterally with 10 µl of saline or 4% capsaicin or 4% formalin into either the whisker pad or the hindpaw, and returned to their home cage. 60–90 min later, mice were anesthetized and underwent stereotaxic surgery for CANE-virus injection. Note that PB is a relatively large area and formalin/capsaicin activated neurons spread along both the dorsal-ventral as well as anterior-posterior axes; while we only injected CANE virus once using one stereotaxic coordinate, so we could only capture some of the neurons. Additionally, injections of formalin/capsaicin in whisker pad on different days could not hit the identical site, and this likely resulted in activation (Fos expression) of overlapping but non-identical populations of PB neurons.

Electrophysiological recording in acute brainstem slices. Four weeks after intraperitoneal injection of AAV9-EF1a-flex-ChR2-eYFP into TrpV1-Cre P1-2 mice, or 3 days after injection of CANE-RV-mCherry into the PB_L of TrpV1-Cre::Ai32;Fos^{TVA} mice, mice were anesthetized with isofluorane, and transcardially

perfused in ice-cold NMDG artificial cerebrospinal fluid (NMDG-ACSF; containing 92 mM NMDG, 2.5 mM KCl, 1.2 mM NaH_2PO_4, 30 mM $NaHCO_3$, 20 mM HEPES, 2 mM glucose, 5 mM sodium ascorbate, 2 mM thiourea, 3 mM sodium pyruvate, 10 mM $MgSO_4$, 0.5 mM $CaCl_2$), and bubbled with 5% CO_2/95% O_2. The brain was then extracted and sectioned into 250 µm thick sagittal slices using a vibratome (VT-1000S, Leica Microsystems) containing ice-cold oxygenated NMDG-ACSF. Sagittal sections including the PB_L were then bubbled in same solution at 37 °C for 8 min, and transferred to bubbled, modified-HEPES ACSF at room temperature (20–25 °C; 92 mM NaCl, 2.5 mM KCl, 1.2 mM NaH_2PO_4, 30 mM $NaHCO_3$, 20 mM HEPES, 2 mM glucose, 5 mM sodium ascorbate, 2 mM thiourea, 3 mM sodium pyruvate, 2 mM $MgSO_4$, 2 mM $CaCl_2$) for at least 1 h before recording. Recordings were performed in a submerged chamber, superfused with continuously bubbled ACSF (125 mM NaCl, 2.5 mM KCl, 1.25 mM NaH_2PO_4, 26 mM $NaHCO_3$, 20 mM glucose, 2 mM $CaCl_2$, 1.3 mM $MgSO_4$) at near-physiological temperature (34 ± 1 °C). Cells expressing GFP were visualized by infrared differential interference contrast and fluorescence video microscopy (Examiner.D1, Zeiss). Whole-cell current clamp recordings were amplified with Multiclamp 700B (filtered at 2 kHz), digitized with Digidata 1440 A (5 kHz), and recorded using pClamp 10 software (Axon). Both unlabeled and mCherry$^+$ PB_L cells surrounded by axon terminals expressing a virally encoded fluorescent marker (ChR2-EYFP) were visualized by infrared differential interference contrast and fluorescence video microscopy (Examiner.D1, Zeiss). Whole-cell voltage-clamp recordings were amplified with Multiclamp 700B (filtered at 2 kHz), digitized with Digidata 1440 A (5 kHz), and recorded using pClamp 10 software (Axon). The patch-clamp electrode (4–6 MΩ) was filled with an intracellular solution containing 130 mM D-gluconic acid, 130 mM CsOH, 5 mM NaCl, 10 mM HEPES, 12 mM phosphocreatine, 3 mM MgATP, 0.2 mM Na_2GTP, 1 mM EGTA. Photostimulation was performed using a 473 nm LED (CoolLED, pE4000) controlled by pClamp 10 software (Axon). Light intensity was set to be 100% for generation of spikes in the axon terminals of projecting TrpV1Cre::ChR2$^+$ neurons with a pulse length of 10 ms. To confirm whether post-synaptic currents were monosynaptic, tetrodotoxin (TTX; 1 µM) was initially bath applied, followed by a combination of TTX and 4-aminopyridine (4-AP; 100 µM).

All electrophysiology data were analyzed off-line using the Neuromatic package (Think Random) in Igor Pro software (WaveMetrics). Off-line analysis was performed by averaging five traces. Light-evoked EPSC and IPSC peak amplitude, half-width, onset latency, time to peak, rise time, and decay time were analyzed. The onset latency of the light-evoked EPSCs and IPSCs was defined as the time from the onset of the stimulus to the first measurable deflection of the potential from the baseline. Similarly, time to peak was defined as the time from the onset of the stimulus to the peak of the potential. Rise time and decay time were defined as the time between 10% and 90% of the rise or decay of the potential, respectively.

Optogenetic activation of TrpV1Cre::ChR2$^+$ sensory afferent terminals in PB_L in a real-time place escape/avoidance (PEA) test and in circular chamber for audio recording. Channelrhodopsin (ChR2) or control GFP was expressed in TrpV1-Cre$^+$ primary sensory neurons by neonatal IP injection of either AAV9-EF1α-DIO-hChR2-eYFP or AAV9-CAG-Flex-GFP in TrpV1-Cre pups (as described above). Six weeks later, virus injected mice were implanted with custom-made optic fibers which were placed above PB-el on both sides and fixed on the skull with dental cement (Parkell). One week later, the animals were subjected to a 2-chamber real-time PEA test in light cycle, using a modified method described previously[55,56]. The size of custom-made behavior chamber is 50.1 × 27.7 × 31.2 cm, made with clear acrylic Plexiglas that had distinct stripe patterns from one another. For optogenetic stimulation, laser is delivered through patch cables attached to the implanted optic fiber as described previously[12]. The mouse is placed in the center of the box and allowed to explore both chambers without light stimulation (pre-stimulation) for 10 min. Generally, after exploration, the mouse shows a small preference for one of the two chambers. Subsequently, blue light stimulation (10 Hz, 20 ms pulse-width, ~3.5 mW) is delivered whenever the mouse enters or stays in the preferred chamber, and light is turned OFF when the mouse moves to the other chamber (stimulation phase, total 10 min). Finally, the mouse can freely explore both chambers without blue light stimulation (post-stimulation) for 10 min. We recorded behavioral data via a webcam (Logitech web-camera, PN 960-000764) interfaced with Bonsai software[57]. Real-time laser stimulation was controlled by Bonsai software through Arduino with a custom-made Arduino sketch (Arduino UNO, A00073). After 1 week, the same group of mice were subjected to another behavioral test, where the mouse was placed in a circular field in a sound proof chamber. The mouse's movements and audible vocalizations were recorded from the top of field using the webcam with audio control at a frame rate 30 fps. The experimental mouse was placed in the center of the circular field and allowed to explore freely. Blue light was delivered as described above. The duration of each light stimulation was 30 s and the interval between light stimuli was > 2 min. The number of light stimulation for each mouse in each behavioral test was 4. The number of pips was calculated for each interval and averaged offline.

After all behavior tests were completed, the mice were given a train of strong light stimulations (15 s on and 15 s off, 50 ms pulses, 10 Hz, ~3.5 mW, repeated 3 times) to elicit ChR2- or photostimulation-dependent Fos expression in their home cage. Subsequently, animals were perfused at 90 min after the final stimulation and processed for Fos immunostaining.

Optogenetic activation of TrpV1Cre::ChR2$^+$ sensory afferent terminals in PB_L in a classical conditioned place aversion (CPA) test. Channelrhodopsin (ChR2) or control GFP was expressed in TrpV1-Cre$^+$ primary sensory by neonatal IP injection of either AAV9-EF1α-DIO-hChR2-eYFP or AAV9-CAG-Flex-GFP in TrpV1-Cre pups (as described above). Six weeks later, virus injected mice were implanted with custom-made optic fibers which were placed above PB-el on both sides and fixed on the skull with dental cement (Parkell). One week later, the animals were subjected to a 2-chamber classic conditioned place aversion (CPA) test in same behavior chamber used for PEA. The mouse is first habituated to the chamber on day 1. On day 2, the mouse is placed in the center of the box and allowed to explore both chambers without light stimulation (pre-stimulation) for 10 min. Generally, after exploration, the mouse shows a small preference for one of the two chambers. In the following two days (day 3 and day 4), the mouse is closed off in the non-preferred chamber with no stimulation for 15 min in the morning, and then closed off in the preferred chamber with blue light stimulation (10 Hz, 20 ms pulse-width, ~3.5 mW) for 15 min in the afternoon. On the final day (day 5), the mouse can explore both chambers without blue light stimulation (post-stimulation) for 10 min, and their behaviors are recorded and analyzed.

Optogenetic silencing of TrpV1Cre::eArch$^+$ sensory afferent terminals in PB_L in von Frey tests and real-time place preference (RTPP) test. Enhanced archaerhodospin (eArch) or control GFP was expressed in TrpV1-Cre$^+$ primary sensory by neonatal IP injection of either AAV9-EF1α-DIO-eARCH-eYFP or AAV9-CAG-Flex-GFP in TrpV1-Cre pups (as described above). Six weeks later, virus injected mice were implanted with custom-made optic fibers which were placed above PB-el on both sides and fixed on the skull with dental cement (Parkell). More than one week later, the animals were subjected to von Frey tests. All mice were first habituated to handling and testing equipment at least 30 min before experiments. Behavioral responses to mechanical stimuli applied to face or hindpaw at baseline (without capsaicin injection) were examined first and both in the absence and in the presence of photo illumination. Subsequently, capsaicin (Sigma-Aldrich, 1 µg/10 µl, dissolved in normal saline with 4% ethanol and 4% Tween-80) was subcutaneously injected into either right hindpaw or right whisker pad. Between 10 and 20 min after capsaicin injection, behavioral responses to mechanical stimuli were tested either in the absence or the presence of photosilencing/illuminating of TrpV1-Cre$^+$ axons in PB_L. The mice were tested for hindpaw and face responses on different days with a randomized order (i.e. some were tested for face first, others were tested for paw responses first). There was at least a one week interval separating the paw versus face (or vice versa) tests. For the hindpaw test, mice were individually placed on an elevated metallic wire mesh floor in polyethylene cages (4 × 4 × 5.5 inch, Comerio-VA, Italy). A graded series of von Frey filaments (0.04–2 g, Stoelting) was inserted through the mesh floor and applied to the plantar surface of the hindpaw. For face test, mice were individually placed in a custom-made box (3 × 3 × 4 inch) with the top, bottom and four walls made of silver wire mesh and allowed for free movement. Again, a graded series of von Frey filaments (0.02–1 g) was inserted through the mesh wells from the lateral side and applied to the skin of the vibrissa pad within the infraorbital nerve territory. A brisk withdrawal of the paw or head was considered a positive response. Mice were tested 3 times with at least 2 withdrawal behaviors out of 3 trials indicating a positive result. Mechanical threshold was defined as the minimum force necessary to elicit a response[58–61]. For optogenetic silencing during von Frey tests, a continuous green light (561 nm) stimulation (~12 mW) was delivered during both the hindpaw and face tests (with and without capsaicin injections). Again, mice were tested 3 times with at least 2 withdrawal behaviors out of 3 trials indicating a positive result. Mechanical threshold was defined as the minimum force necessary to elicit a response.

TrpV1Cre::eArch and TrpV1Cre::GFP mice were also subjected to a real-time place preference test (RTPP). An individual mouse was placed in the center of the box and allowed to explore both chambers without light stimulation (baseline) for 10 min. Generally, after exploration, the mouse shows a small preference for one of the two chambers. After recording the baseline behavior, individual mouse was injected with 5 µl 4% capsaicin into the left whisker pad and placed in the chamber again to freely explore both chambers without light stimulation (no stimulation) for 10 min again. Subsequently, a continuous green light stimulation (561 nm, ~12 mW) was delivered through the optic fiber to silence the TrpV1Cre::eArch$^+$ fibers (or illuminate the control GFP$^+$ fibers) in PB_L whenever the mouse entered or stayed in the non-preferred chamber, and light was turned off when the mouse moved to the other chamber (total 10 min of real-time stimulation). We recorded behavioral data via a webcam (Logitech web-camera, PN 960-000764) interfaced with Bonsai software[57]. Real-time laser stimulation was controlled by Bonsai software through Arduino with a custom-made Arduino sketch (Arduino UNO, A00073). Subsequently, animals were perfused for post-hoc analysis.

Statistics. No statistical methods were used to predetermine sample sizes, but our sample sizes are similar to those reported in previous publications[12,62,63]. Values in text are reported as mean ± s.e.m. All data (with the exception of behavioral data

for the real-time PEA test) were analyzed using two-tailed paired and unpaired Student's *t* test between 2 groups (experimental or control), or in the case of multiple groups, one-way or two-way ANOVA followed by Tukey's test. The criterion for statistical significance was $P < 0.05$. Regarding the assumption of normality for large/medium datasets, D'Agostino and Pearson normality test was used. When the sample size was less than four, Shapiro-Wilk normality test was used. We provide mean values with associated s.e.m. values. To determine whether the variance was similar between the groups that are being statistically compared, *F* test was used for *t* tests, and Brown-Forsythe was used for one-way ANOVA. The results showed that the variance was similar.

Behavioral data for real-time PEA and RTPP tests were analyzed using one-way repeated measures ANOVA with Matlab R2016a. The statistical test was used for ChR2 group and GFP group independently. For PEA, the preference of the stimulation side between PRE (no-stim), STIM, and POST (no-stim) periods was compared. For RTPP, the preference of the stimulation side between Baseline, No Stimulation, and Stimulation periods was compared. Tukey's test was used post-hoc. Behavioral data for von Frey tests were analyzed using two-way repeated measures ANOVA. The statistical test was used for face test and hindpaw test independently. For both tests, both between and within eArch and GFP groups across conditions were compared.

Life Sciences Reporting Summary. Further information on experimental design and reagents is available in the Life Sciences Reporting Summary.

Data availability. The data collected in this study are available from the corresponding author upon request.

Code availability. All custom-written MatLab code used in this study is available at https://github.com/wanglab-duke/craniofacial-specific-monosynaptic-circuit-for-affective-pain.

nature research

Corresponding author(s): Fan Wang

☐ Initial submission ☐ Revised version ☒ Final submission

Life Sciences Reporting Summary

Nature Research wishes to improve the reproducibility of the work that we publish. This form is intended for publication with all accepted life science papers and provides structure for consistency and transparency in reporting. Every life science submission will use this form; some list items might not apply to an individual manuscript, but all fields must be completed for clarity.

For further information on the points included in this form, see Reporting Life Sciences Research. For further information on Nature Research policies, including our data availability policy, see Authors & Referees and the Editorial Policy Checklist.

Experimental design

1. Sample size

   Describe how sample size was determined.

   No statistical methods were used to pre-determine sample sizes, but our sample sizes are similar to those reported in previous publications (reference 28)

2. Data exclusions

   Describe any data exclusions.

   For behavioral experiments, we used two exclusion criteria for our subjects: (1) poor recovery or other health concerns following surgical intervention or (2) missed injection or implantation target, as determined by posthoc histological analysis. Animals were randomly selected from each litter.

   For axonal tracing experiments, ROI's with densities in which the total pixel numbers of GFP-labeled axons divided by the area of the nuclei was less than 0.1 were not counted.

3. Replication

   Describe whether the experimental findings were reliably reproduced.

   All experimental findings were reliably reproduced among all subjects in all experiments. This is reported throughout all the figure legends.

4. Randomization

   Describe how samples/organisms/participants were allocated into experimental groups.

   Animals were randomly selected from each litter. Random group allocation was maintained throughout the study, within constraints set by availability of in-house, purpose-bred lines.

5. Blinding

   Describe whether the investigators were blinded to group allocation during data collection and/or analysis.

   Investigators were blinded to group allocation during data collection and during data analysis. Behavioral analysis relied on objective, automatized measurements.

Note: all studies involving animals and/or human research participants must disclose whether blinding and randomization were used.

6. Statistical parameters

For all figures and tables that use statistical methods, confirm that the following items are present in relevant figure legends (or in the Methods section if additional space is needed).

n/a	Confirmed
☐	☒ The exact sample size (*n*) for each experimental group/condition, given as a discrete number and unit of measurement (animals, litters, cultures, etc.)
☐	☒ A description of how samples were collected, noting whether measurements were taken from distinct samples or whether the same sample was measured repeatedly
☐	☒ A statement indicating how many times each experiment was replicated
☐	☒ The statistical test(s) used and whether they are one- or two-sided (note: only common tests should be described solely by name; more complex techniques should be described in the Methods section)
☐	☒ A description of any assumptions or corrections, such as an adjustment for multiple comparisons
☐	☒ The test results (e.g. *P* values) given as exact values whenever possible and with confidence intervals noted
☐	☒ A clear description of statistics including central tendency (e.g. median, mean) and variation (e.g. standard deviation, interquartile range)
☐	☒ Clearly defined error bars

See the web collection on statistics for biologists for further resources and guidance.

Software

Policy information about availability of computer code

7. Software

Describe the software used to analyze the data in this study.

We recorded all behavioral data via a webcam (Logitech web-camera, PN 960-000764). We recorded all place preference and avoidance data via a webcam interfaced with Bonsai software . Real-time laser stimulation was controlled by Bonsai software through Arduino with a custom-made Arduino sketch.

Matlab 2016a was used to analyze axonal projections and mouse movements for place preference and avoidance tests.

FIJI (image J) were used to count the number of cells in various experiments.

Igor pro was used to analyze electrophysiological data.

GraphPad Prism 7 was used for statistical analysis and graphing the results.

For manuscripts utilizing custom algorithms or software that are central to the paper but not yet described in the published literature, software must be made available to editors and reviewers upon request. We strongly encourage code deposition in a community repository (e.g. GitHub). *Nature Methods* guidance for providing algorithms and software for publication provides further information on this topic.

Materials and reagents

Policy information about availability of materials

8. Materials availability

Indicate whether there are restrictions on availability of unique materials or if these materials are only available for distribution by a for-profit company.

n/a

9. Antibodies

Describe the antibodies used and how they were validated for use in the system under study (i.e. assay and species).

Goat anti-Fos (Santa Cruz Biotechnology, sc52-g, 1:300), rabbit anti-CGRP (Millipore, AB15360, 1:1000), sheep anti-FoxP2 (R&D Systems, AF5647, 1:5000), rabbit anti-NF200 (Sigma, N4142, 1:200), GS-IB4-Alexa 488–conjugated (Invitrogen, I21411, 1:1000), rabbit anti-VR1 (Abcam, ab31895, 1:1000), and rabbit anti-GFP (Abcam, ab290, 1:1000). The secondary antibodies are: Alexa Fluor 488 donkey anti-goat (Jackson immunoresearch, 705-545-147 1:1,000), Cy3 donkey anti-goat (Jackson immunoresearch, 705-165-147, 1:1,000), Alexa Fluor 488 donkey anti-rabbit (Jackson immunoresearch, 703-545-155, 1:1,000), Cy3 donkey anti-rabbit (Jackson immunoresearch, 711-165-152, 1:1,000), and Alexa Fluor 488 donkey anti-sheep (Abcam, ab150181, 1:1000).
For each primary antibody, we cited a reference.

10. Eukaryotic cell lines

a. State the source of each eukaryotic cell line used. n/a

b. Describe the method of cell line authentication used. n/a

c. Report whether the cell lines were tested for mycoplasma contamination. n/a

d. If any of the cell lines used are listed in the database of commonly misidentified cell lines maintained by ICLAC, provide a scientific rationale for their use. n/a

Animals and human research participants

Policy information about studies involving animals; when reporting animal research, follow the ARRIVE guidelines

11. Description of research animals

Provide details on animals and/or animal-derived materials used in the study. Adult (p30-p60) male and female C57/BL6, FosTVA, TrpV1-Cre, Ai32 & Ai65D mice.

Policy information about studies involving human research participants

12. Description of human research participants

Describe the covariate-relevant population characteristics of the human research participants. n/a